

Lawrence Berkeley National Laboratory

LBL Publications

Title

Influences of Hillslope Biogeochemistry on Anaerobic Soil Organic Matter Decomposition in a Tundra Watershed

Permalink

<https://escholarship.org/uc/item/5gg1k6zm>

Journal

Journal of Geophysical Research Biogeosciences, 125(7)

ISSN

2169-8953

Authors

Philben, Michael
Taş, Neslihan
Chen, Hongmei
[et al.](#)

Publication Date

2020-07-01

DOI

10.1029/2019jg005512

Peer reviewed

1 **Influences of hillslope biogeochemistry on anaerobic soil organic matter decomposition in a**
2 **tundra watershed**

3

4 M. Philben^{1*}, N. Taş², H. Chen³, S. D. Wullschleger¹, A. Kholodov⁴, D. E. Graham⁵, and B. Gu¹

5 ¹Environmental Sciences Division, Oak Ridge National Laboratory

6 ²Climate and Ecosystem Sciences Division, Lawrence Berkeley National Laboratory

7 ³Department of Chemistry and Biochemistry, Old Dominion University

8 ⁴Geophysical Institute, University of Alaska Fairbanks

9 ⁵Biosciences Division, Oak Ridge National Laboratory

10 *Present address: Department of Geology and Environmental Science, Hope College

11 Corresponding authors: Michael Philben (philben@hope.edu) and Baohua Gu (gub1@ornl.gov)

12 **Key Points:**

- 13
- 14 • We compared CO₂ and CH₄ production in soils from two wetland areas along a tundra hillslope gradient (toeslope and peat plateau).
 - 15 • Production of both gasses was higher in the organic toeslope soils, while microbial N
 - 16 limitation was higher in peat plateau soils.
 - 17 • Downslope transport of N, DOM, and alkalinity increases greenhouse gas production in
 - 18 the organic toeslope soils.
 - 19

20 **Abstract**

21 We investigated rates and controls on greenhouse gas (CO₂ and CH₄) production in two
22 contrasting water-saturated tundra soils within a permafrost-affected watershed near Nome,
23 Alaska, United States. Three years of field sample analysis have shown that soil from a fen-like
24 area in the toeslope of the watershed had higher pH and higher porewater ion concentrations than
25 soil collected from a bog-like peat plateau at the top of the hillslope. The influence of these
26 contrasting geochemical and topographic environments on CO₂ and CH₄ production was tested
27 in soil microcosms by incubating both the organic- and mineral-layer soils anaerobically for 55
28 days. Nitrogen (as NH₄Cl) was added to half of the microcosms to test potential effects of N
29 limitation on microbial greenhouse gas production. We found that the organic toeslope soils
30 produced more CO₂ and CH₄, fueled by higher pH and higher concentrations of water-
31 extractable organic C (WEOC). Our results also indicate N limitation on CO₂ production in the
32 peat plateau soils, but not the toeslope soils. Together these results suggest that the weathering
33 and leaching of ions and nutrients from tundra hillslopes can increase the rate of anaerobic soil
34 organic matter decomposition in downslope soils by (1) increasing the pH of soil porewater; (2)
35 providing bioavailable WEOC and fermentation products such as acetate; and (3) relieving
36 microbial N limitation through nutrient runoff. We conclude that the soil geochemistry as
37 mediated by landscape position is an important factor influencing the rate and magnitude of
38 greenhouse gas production in tundra soils.

39 **1 Introduction**

40 Hillslope topography organizes the distribution of water, energy, and nutrients within
41 landscapes (Burt & Pinay, 2005). Erosion and selective leaching from areas with elevated
42 topography results in gradients of soil grain size, composition and chemistry (Milne, 1936;
43 Moore et al., 1993; Wang et al., 2009). This typically results in the accumulation of soil organic

44 matter (SOM), nutrients, and other soil-derived solutes in low-lying areas within watersheds
45 (Creed et al., 2002; Yoo et al., 2006), provided that the soils are hydrologically connected
46 (Hornberger et al., 1994; Stieglitz et al., 2003). In temperate watersheds, slope and elevation
47 have been successfully used to predict stocks of SOM, soil pH, and nutrient concentrations
48 (Creed et al., 2002; Hall & Olson, 1991; Moore et al., 1993). There is therefore growing interest
49 in representing hillslope processes as sub-grid cell heterogeneity in the next generation of Earth
50 system models (Fan et al., 2019).

51 Accurately representing these processes in the Arctic is particularly important because Arctic
52 soils contain about one-third of the total global C pool (Hugelius et al., 2014; Schuur et al., 2015)
53 and are severely under-studied compared to temperate soils (Metcalfe et al., 2018). There is
54 evidence that similar geochemical gradients exist on Arctic hillslopes, in that nutrients, soil
55 organic matter (SOM), and leachable cations accumulate in low-lying soils (Koch et al., 2014;
56 Lev & King, 1999; Stewart et al., 2014; Yano et al., 2010). However, the presence of permafrost
57 underlying many Arctic soils impedes drainage (Liljedahl et al., 2016). This isolates surface
58 water from deeper flow pathways and increases the hydrological connectivity of the surface
59 soils, potentially strengthening the relationship between the chemistry of the ridge and valley
60 surface soils (Bring et al., 2016). In addition, poor drainage results in saturated soils in upland
61 areas as well as lowlands. Therefore, we expect a trend of increasing pH and increasing nutrient
62 concentrations in low-lying soils compared to uplands due to erosion, selective leaching, and
63 weathering.

64 Previous studies suggest these environmental variables are important regulators of CO₂ and
65 CH₄ emission from SOM decomposition. For example, rates of anaerobic SOM decomposition in
66 boreal peatlands are consistently observed to increase along gradients of groundwater inputs,

67 from precipitation-fed bogs to mineral-rich fens (Keller et al., 2006; Thormann et al., 1999). This
68 pattern has been attributed both to higher alkalinity via weathering (Ye et al., 2012) and nutrient
69 availability (Bayley et al., 2005; Keller et al., 2006) provided by groundwater inputs. Studies of
70 tundra soils have also indicated that CH₄ production is sensitive to pH (Tang et al., 2016; Zheng
71 et al., 2019a), nutrients (Philben et al., 2019), and the concentration of labile organic matter
72 (Chen et al., 2018; Yang et al., 2016). Here, we test the hypothesis that the variability in pH and
73 nutrient availability over a permafrost-affected Arctic hillslope constitutes a landscape-level
74 influence over the rate and pathways of SOM decomposition.

75 We used laboratory microcosm incubations to investigate differences in potential anaerobic
76 SOM decomposition between two wetland areas within an Arctic watershed near Nome, Alaska.
77 Both are characterized by wet sedge tussock tundra plant community, organic-rich soils, and
78 water tables near the soil surface during the thaw season (Jafarov et al., 2018). However, field
79 observations revealed that their positions on opposite ends of the hillslope results in contrasting
80 porewater geochemistry. We hypothesized that these geochemical differences affect the rates and
81 pathways of anaerobic SOM decomposition, specifically that the transport of leached ions,
82 nutrients, and dissolved organic matter down the hillslope fuels greenhouse gas production in the
83 low-lying toeslope compared to elevated plateau.

84 **2 Materials and Methods**

85 **2.1 Study site**

86 Soil cores and porewater were collected from two locations within the same watershed in
87 the Teller Road mile 27 site of the Next Generation Ecosystem Experiment (NGEE)-Arctic
88 project (<http://ngee-arctic.ornl.gov>). The site is located in hilly terrain in the southern Seward
89 Peninsula, Alaska, on a southeast-facing hillslope (Jafarov et al., 2018). One site (hereafter

90 “Plateau”) is located on the peat plateau on the top of the hillslope (N64.74512° W165.96668°,
91 WGS84 datum), and the other site (“Toeslope”) from the wetland in the toeslope (N64.72946°
92 W165.94465°). Both sites are characterized by tussock tundra, sedge-dominated vegetation, and
93 a water table at or near the soil surface. The depth of the permafrost table varies with hillslope
94 position: the thick peat layers in the peat plateau insulate the soil, resulting in near-surface
95 permafrost, while the active layer is thicker on the hillslope due to greater snow accumulation
96 (Jafarov et al., 2018). The toeslope consists of a collapsed peat plateau wetland that lacks near-
97 surface permafrost (> 1 m thaw depth in August 2018). In August 2018 the surface water
98 temperature was 10 °C.

99

100 2.2 Soil and porewater collection

101 Porewater samples were collected from the two sites on five occasions over three years
102 (September 9 and 13, 2016; August 9, 2017; September 10, 2017; and August 22, 2018).

103 Samples were collected using PVC piezometers with slits cut into the sides 10–15 cm from the
104 bottom to allow soil porewater to percolate in while excluding soil particles. Piezometers were
105 installed at depths of approximately 35 and 70 cm to sample the organic and mineral soils,
106 respectively. pH was measured in the field using a Hanna Instruments portable pH meter.

107 Subsamples for cation analyses were returned to the laboratory and analyzed using inductively
108 coupled plasma mass spectrometry (ICP-MS). The full dataset from these field measurements
109 (Zheng et al., 2019b) is available in the NGEE-Arctic data portal ([https://ngee-
110 arctic.ornl.gov/data](https://ngee-arctic.ornl.gov/data)).

111 Cores from the two sites were collected on June 1, 2017 prior to the thawing of the active
112 layer. Frozen cores were collected using an AMS Frozen Soil Powered Auger. Soil cores (5.1 cm

113 diameter) were removed from the unlined auger barrel, wrapped in plastic sleeve, and cooled
114 with freezer packs. The peat plateau core was drilled at location N64.74514° W165.96651° while
115 the toeslope core was from W64.729193°, W165.944072°. The core from the plateau was 76 cm
116 in length, and the toeslope core was 84 cm. The cores were shipped frozen to Oak Ridge
117 National Laboratory and stored frozen until the start of the incubation. The frozen cores were
118 transferred to an anaerobic chamber and separated into organic and mineral soil layers based on
119 visual inspection. The uppermost layers containing intact vegetation were removed. The 0-38 cm
120 and 0-34 cm intervals were characterized as organic for the toeslope and the plateau,
121 respectively. Core sections from 38-84 cm for the toeslope and 61-76 cm for the plateau were
122 used for the mineral soil.

123

124 2.3 Microcosm construction

125 The separated cores were cut into small ($<0.5 \text{ cm}^3$) pieces using an oscillating cutting tool
126 and mixed with a spoon, creating four homogenized samples (organic and mineral soils for the
127 toeslope and the plateau). Soil microcosms were constructed by adding 7 g (wet soil) to 60 mL
128 serum bottles. 1 mL of either deionized water (control treatment) or NH_4Cl solution containing
129 32 mM N (+N treatment) was added to each microcosm, so that the amendment would increase
130 the concentration of inorganic N by approximately 10-fold, based on previous measurements of
131 N in the toeslope soil (Philben et al., 2019). Three replicate microcosms were prepared for the
132 control and +N treatments to be incubated at -2°C and 8°C for 55 days. In addition, three
133 replicates were constructed for destructive sampling and soil microbial analyses after 15 and 30
134 days for the 8°C treatment only. The microcosms were sealed with blue rubber septa, crimped

135 with aluminum caps, headspace flushed with N₂ for 10 minutes, and transferred to incubators at
136 the appropriate temperature.

137

138 2.4 Greenhouse gas and chemical analysis

139 Concentrations of CO₂ and CH₄ were measured in the headspace of the microcosms every
140 two days for the first two weeks, then every five days thereafter. On each sampling day, 0.5 mL
141 of the headspace was analyzed using gas chromatography, as previously described (Roy
142 Chowdhury et al., 2015). The microcosms incubated at -2°C were kept in a cooler filled with ice
143 packs during analysis to reduce temperature change during the incubation. Headspace CO₂ and
144 CH₄ concentrations were converted to total gas production using Henry's Law based on the
145 water content, temperature of incubation and measured soil pH (Sander, 2015). Gas production
146 was normalized to per g dry weight (gdw⁻¹) of the soil to compare between soils with variable
147 water contents.

148 Microcosms were destructively sampled after 15, 30, and 55 days of incubation. In an
149 anaerobic chamber, 2 g of each soil was extracted with 10 mL of degassed water or 0.1 M KCl in
150 a 15 mL plastic tube and placed on a reciprocal shaker for 90 minutes. The soil extracts were
151 centrifuged for 10 min and filtered through a 0.2 µm syringe filter. Aliquots of the KCl extracts
152 were analyzed immediately for pH and Fe(II) using the 1,10-phenanthroline method (Hach
153 method 8146). NH₄-N concentrations were also analyzed in the KCl extracts using the
154 colorimetric salicylate and cyanurate method (Hach method 10031).

155 The water extracts were analyzed for major anion content, low-molecular weight organic
156 acid concentration, UV-visible absorbance, and water-extractable organic C (WEOC). Samples
157 were either analyzed within three days of collection or frozen until analysis. Specifically, anions

158 (Cl⁻, Br⁻, NO₃⁻, and SO₄²⁻) and organic acids (formate, acetate, propionate, butyrate, and oxalate)
159 were analyzed in the water extracts using ion chromatography using previously established
160 methods (Herndon et al. 2015). The ions were separated using a 4 µm Dionex IonPac AS11-HC
161 column and gradient elution. The eluent was 1 mM KOH from 0-7 min, ramping to 15 mM from
162 7-16 min, 30 mM at 25 min, and 60 mM at 33 min. Ions were detected using a Dionex
163 suppressed conductivity detector.

164 Water-extractable organic carbon (WEOC) concentration in the soil extracts were
165 analyzed using a Shimadzu TOC-L analyzer after acidification with 0.1% HCl and purging to
166 remove inorganic C (CO₃²⁻ and HCO₃⁻). Ultraviolet-visible (UV-Vis) spectroscopy was also
167 conducted on the water extracts in a 1 cm quartz cuvette over the range 200–800 nm on a
168 Hewlett-Packard 8453 spectrophotometer. Specific UV absorptivity at 254 nm (SUVA₂₅₄) was
169 calculated as:

$$\text{SUVA}_{254} = 100 \times \frac{A_{254}}{[\text{WEOC}]}$$

170 where A_{254} indicates the absorbance at 254 nm and [WEOC] is the WEOC concentration in mg C
171 L⁻¹ (Weishaar et al., 2003).

172

173 2.5 FTICR-MS analysis of DOM molecular composition

174 Selected samples from Day 0 and Day 55 of the incubation were analyzed using Fourier
175 transform ion cyclotron resonance mass spectrometry (FTICR-MS). The WEOC fraction was
176 subjected to solid-phase extraction (SPE) using Bond Elut PPL cartridges (Agilent) following a
177 method developed by Dittmar et al. (2008). Sample volumes of approximately 5 mL at an
178 average DOC concentration of 35 ± 20 mg L⁻¹ were acidified with HCl to pH ~2, and loaded
179 onto PPL cartridges (3 mL, 0.1 gram of resin), which were conditioned with LC-MS grade

180 methanol (Fisher Scientific) before use. PPL cartridges after desalting were dried by flushing
181 with ultra-purity nitrogen gas and DOM was eluted out with 1–2 mL of LC-MS grade methanol.
182 The eluate was then stored at -20 °C until FTICR-MS measurements. Samples were analyzed
183 using a Bruker Daltonics 12 Tesla Apex Qe FTICR-MS interfaced to an Apollo electrospray
184 ionization (ESI) source operating in the negative ion mode. Prior to analysis, DOM extracts and
185 PPL blanks were diluted with LC-MS grade water to a methanol:water ratio of 1:1. Samples
186 were injected into the ESI source at an infusion rate of 120 $\mu\text{L h}^{-1}$. The ESI spray current was
187 stable at approximately 20 nA for all sample runs. Ion accumulation in the hexapole was set to
188 3.0 seconds, and 300 transients were co-added and digitized with a 4 M Word data acquisition
189 size.

190 FTICR-MS was externally calibrated with a polyethylene glycol standard and internally
191 calibrated with naturally present homologous series of organic acids detected within samples
192 (Chen et al., 2018). Peaks detected in experimental blanks were removed from the DOM peak
193 list. Molecular formulas were assigned to peaks with a signal to noise (S/N) above 4, using the
194 molecular formula calculator from the National High Magnetic Field Laboratory (Molecular
195 Formula Calc v.1.0 © NHML, 1998). The criteria were set as $^{12}\text{C}_{2-50}$, $^1\text{H}_{2-120}$, $^{16}\text{O}_{0-30}$, $^{14}\text{N}_{0-10}$,
196 $^{32}\text{S}_{0-2}$, $^{34}\text{P}_{0-1}$, where the subscripts show the range of atoms allowed in each formula. The
197 majority (>95%) of the assigned formulas were within 0.5 ppm mass accuracy, and all formulas
198 were within 1.0 ppm mass accuracy. Molecules were categorized by compound class using
199 chemical composition metrics as described previously (Chen et al., 2018). Briefly, double bond
200 equivalent (DBE) values are calculated as $\text{DBE} = 1 + \text{C} - 0.5\text{H} + 0.5 \text{N} + 0.5 \text{P}$. The modified
201 aromaticity index (AI_{mod}) was calculated as $\text{AI}_{\text{mod}} = (1 + \text{C} - 0.5\text{O} - \text{S} - 0.5\text{N} - 0.5 \text{P} - 0.5\text{H})/(\text{C}$

202 – 0.5O – N – S – P), which indicates aromatics when the value is ≥ 0.5 , or condensed aromatics
203 when the value is ≥ 0.67 (Koch & Dittmar, 2006).

204

205 2.6 Microbial community analysis

206 Total DNA was extracted from Day 0 and Day 55 microcosms by using 0.25 g of wet soil as
207 input to the DNeasy PowerSoil Kit (Qiagen, Germantown, MD, USA) with minor modifications.
208 Prior to bead-beating, the samples were incubated in bead-solution at 65 °C for 5 min. Samples
209 were disrupted by bead beating with a 1600 MiniG (SPEX Sample Prep, Metuchen, NJ, USA) at
210 a setting of 1500 rpm for 60 s and the DNA was further purified according to the kit protocol.
211 16S rRNA genes were amplified in PCR reactions using primers (F515/R806) that target the V4
212 region of the 16S rRNA gene where reverse PCR primer was barcoded with a 12-base Golay
213 code (Caporaso et al., 2010). The PCR reactions contained 2.5 μ l Takara Ex Taq PCR buffer, 2
214 μ l Takara dNTP mix, 0.7 μ l Roche BSA (20 mg/ml), 0.5 μ l each of the forward and reverse
215 primers (10 μ M final concentration), 0.125 μ l Takara Ex Taq Hot Start DNA Polymerase
216 (TaKaRa, Shiga, Japan), 1.0 μ l genomic DNA (10 ng/reaction), and nuclease-free water in a total
217 volume of 25 μ l. Reactions were held at 98 °C for 3 min to denature the DNA, followed by
218 amplification for 25 cycles at 98 °C for 30 s, 52 °C for 30 s, and 72 °C for 60 s, and a final
219 extension of 12 min at 72 °C. Each sample was amplified in triplicate, combined, and purified
220 using the Agencourt AMPure XP PCR purification system (Beckman Coulter, Brea, CA). The
221 purified amplicons were quantified using the Qubit dsDNA HS assay (Invitrogen, Carlsbad, CA,
222 USA). Amplicons were pooled (10 ng/sample) and sequenced on one lane of the Illumina Miseq
223 platform (Illumina Inc, San Diego, CA) resulting in 300 bp paired-end reads. Sequence data are
224 deposited at European Nucleotide Archive with accession PRJEB34184.

225 Paired-end amplicon sequences were overlapped and merged using FLASH (Magoč &
226 Salzberg, 2011). Quality filtering and demultiplexing were performed as described previously
227 (Bokulich et al., 2013). Sequences were grouped into operational taxonomic units (OTUs) based
228 on 97% sequence identity, and chimeric sequences were removed using UPARSE (Edgar, 2013).
229 For 16S rRNA gene analysis, OTUs were given taxonomic assignments in QIIME (Caporaso et
230 al., 2010) version 1.7.0 using the RDP classifier (Wang et al., 2007) and the SILVA database 132
231 (Quast et al., 2013). Phylogenetic trees were created using FastTree (Price et al., 2010) under
232 QIIME's default parameters. All remaining analysis were performed in R version 3.5.1 (Bates et
233 al., 2014; R Core Team, 2013) via use of phyloseq (McMurdie & Holmes, 2013), vegan
234 (Oksanen et al., 2013) and ggstatsplot (Patil et al., 2019) packages. Amplicon data were
235 proportionally normalized, and β -diversity was assessed by perMANOVA (Anderson & Walsh,
236 2013) using Bray-Curtis distance (Bray & Curtis, 1957). For multiple comparisons p values were
237 adjusted via Bonferroni method.

238

239 2.7 Statistical analysis

240 Porewater chemistry data were fit to a linear mixed effects model using the package lme4 in
241 R version 3.5.1 (Bates et al., 2014; R Core Team, 2013). Time of incubation (0, 30, or 55 days)
242 and treatment (control or +N) were used as fixed factors, and the microcosm replicate was used
243 as a random factor to account for the effects of repeated sampling. The treatment effect was
244 excluded from the model for the inorganic N ($\text{NO}_3^- + \text{NH}_4^+$) measurements so that temporal
245 changes in the control treatments were evaluated. For the CO_2 and CH_4 measurements, the
246 difference between concentrations at 29 and 50 days in the Control and +N treatments were
247 compared using the mixed effects model. Note that the days analyzed are different for the

248 greenhouse gas concentrations and porewater chemistry due to differences in their respective
249 sampling intervals. A separate ANOVA analysis was performed using the R base package to
250 evaluate differences in initial soil porewater chemistry among the four soils. A significance
251 threshold of $p=0.05$ was used for all statistical analyses.

252 **3 Results**

253 3.1 Porewater geochemistry of field samples

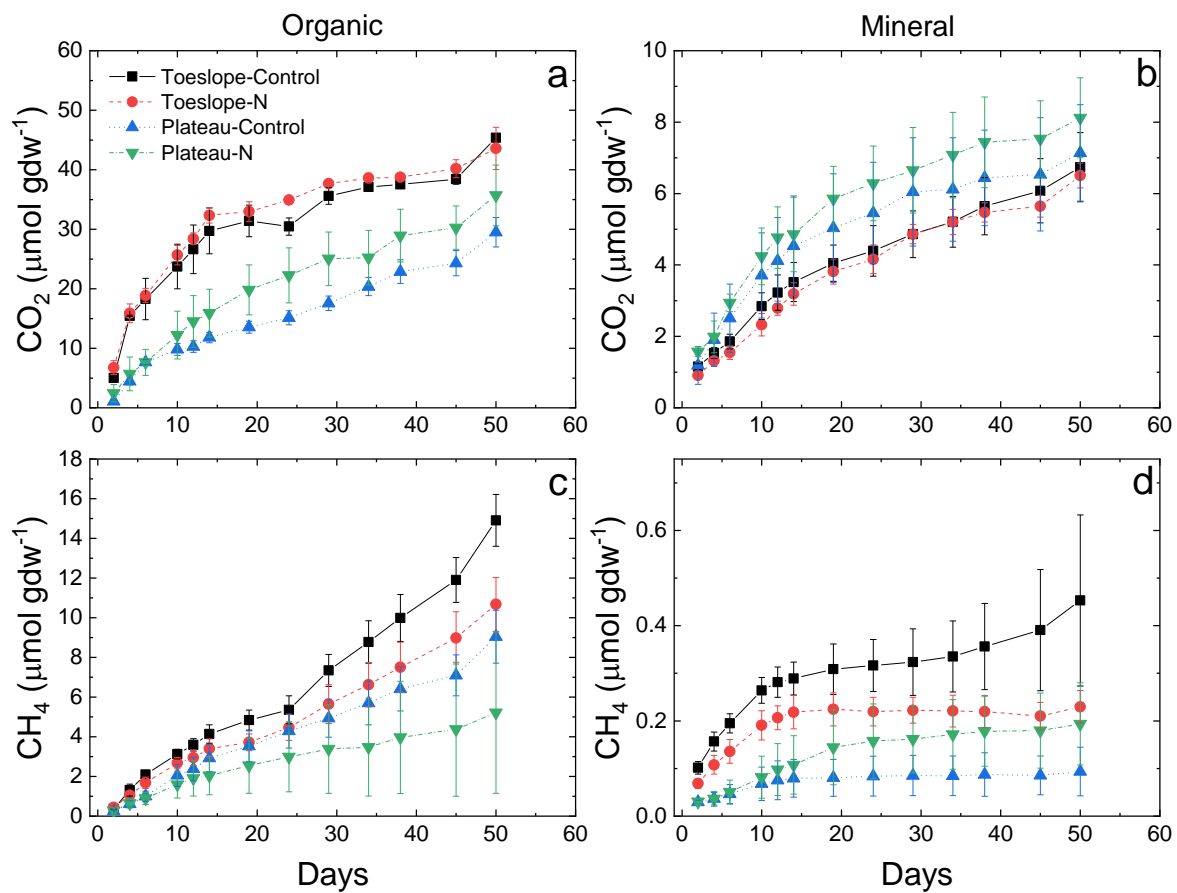
254 Comparison of the soil porewater geochemistry over five sampling time points indicated that
255 the average pH was approximately 1 pH unit higher in the toeslope soils than the plateau soils.
256 This was observed in both the organic soil (6.73 and 5.59, respectively; Fig. S1) and in the
257 mineral soils (6.62 and 5.86, respectively). The mean concentration of dissolved cations was also
258 higher and contained a higher proportion of alkali earth metals in the toeslope, consistent with
259 the input of weathering products from the hillslope. The mean molar ratio of alkali to alkali Earth
260 cations was 1.34 and 2.20 in the organic and mineral soils of the plateau, respectively, compared
261 to 0.11 and 0.08 in the organic and mineral soils of the toeslope (Fig. S1).

262

263 3.2 Rates and temperature sensitivity of greenhouse gas production

264 CO_2 production at both sites was higher in the organic soils than the mineral soils (Fig.
265 1a,b). It was higher in the organic soils of the toeslope than the organic soils of the plateau,
266 especially during the first 15 days of incubation (Fig. 1a; $p<0.001$). CO_2 production was not
267 significantly different between the two mineral soils. Similar to the patterns for CO_2 production,
268 CH_4 production was significantly higher in the toeslope soils than in the plateau soils in the
269 organic ($p=0.047$) but not the mineral soils (Fig. 1c,d), which produced low levels of CH_4 .

270 N addition had contrasting effects on CO₂ and CH₄ production, as effects on CO₂ varied
 271 by soil but CH₄ production was generally inhibited (Fig. 2). N addition had no effect on CO₂
 272 production in either the organic or mineral soils from the toeslope. However, it significantly
 273 increased CO₂ production in the organic plateau soils (p=0.010). N addition also increased CO₂
 274 production in the plateau mineral soils, but the difference was not significant. In contrast, N
 275 addition generally reduced CH₄ production in all soils except for the plateau mineral soil, which
 276 exhibited a small but not significant increase. However, the effect on decreasing CH₄ production
 277 was significant only for the toeslope soils (p=0.004 and 0.024 for the organic and mineral soils,
 278 respectively).



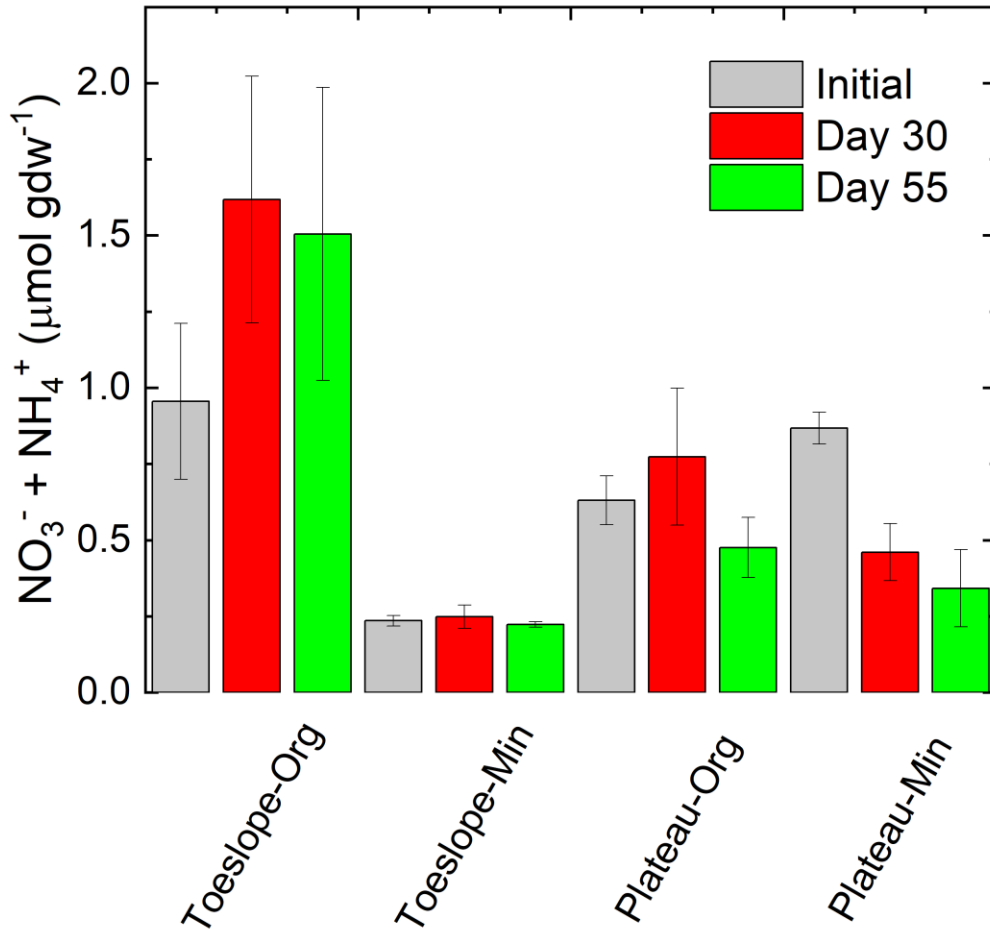
279

280 **Figure 1.** Cumulative CO₂ (a,b) and CH₄ (c,d) production in the incubations of two contrasting
281 water-saturated tundra soils within a watershed near Nome, Alaska. Incubations were performed
282 with both the organic and mineral layer soils either with or without addition of inorganic N (as
283 NH₄Cl). Symbols indicate the mean of three replicates and error bars indicate one standard
284 deviation. Abbreviation “gdw” refers to g dry weight soil.

285

286 3.3 N dynamics

287 The extractable inorganic N content (the sum of independently measured NO₃⁻ and NH₄⁺)
288 of the organic soil was higher in the toeslope than the plateau soils (0.96 and 0.63 μmol N gdw⁻¹,
289 respectively; p=0.020; Fig. 2). The opposite pattern was observed in the mineral soils (p=0.001).
290 However, both plateau soils exhibited net N immobilization (i.e. the concentration of extractable
291 inorganic N significantly declined during the incubation; p < 0.001). The toeslope soils both
292 exhibited net N mineralization (increased extractable inorganic N) but the change was not
293 significant. Inorganic N concentrations in the +N treatment soils declined during incubation for
294 all four soils, indicating microbial uptake or gaseous loss. The decline in concentration was
295 similar for the two organic soils (4.4 and 4.2 μmol gdw⁻¹ for the toeslope and plateau,
296 respectively), and was greater than that in the mineral soils (3.3 and 2.3 μmol gdw⁻¹,
297 respectively).



298

299 **Figure 2.** Total extractable inorganic N ($\text{NH}_4^+ + \text{NO}_3^-$) in the initial soils and after 30 and 55
 300 days of incubation. The height of the bars indicate the mean of three replicates and the error bars
 301 indicate one standard deviation.

302

303

304

305 3.4 WEOC quantity and composition

306 Initial concentrations of WEOC were higher in the toeslope than the plateau in both the

307 organic and mineral soils (Fig. 3a,b; $p < 0.001$). WEOC concentrations significantly declined

308 during incubation in all soils ($p < 0.001$), indicating decomposition and immobilization of

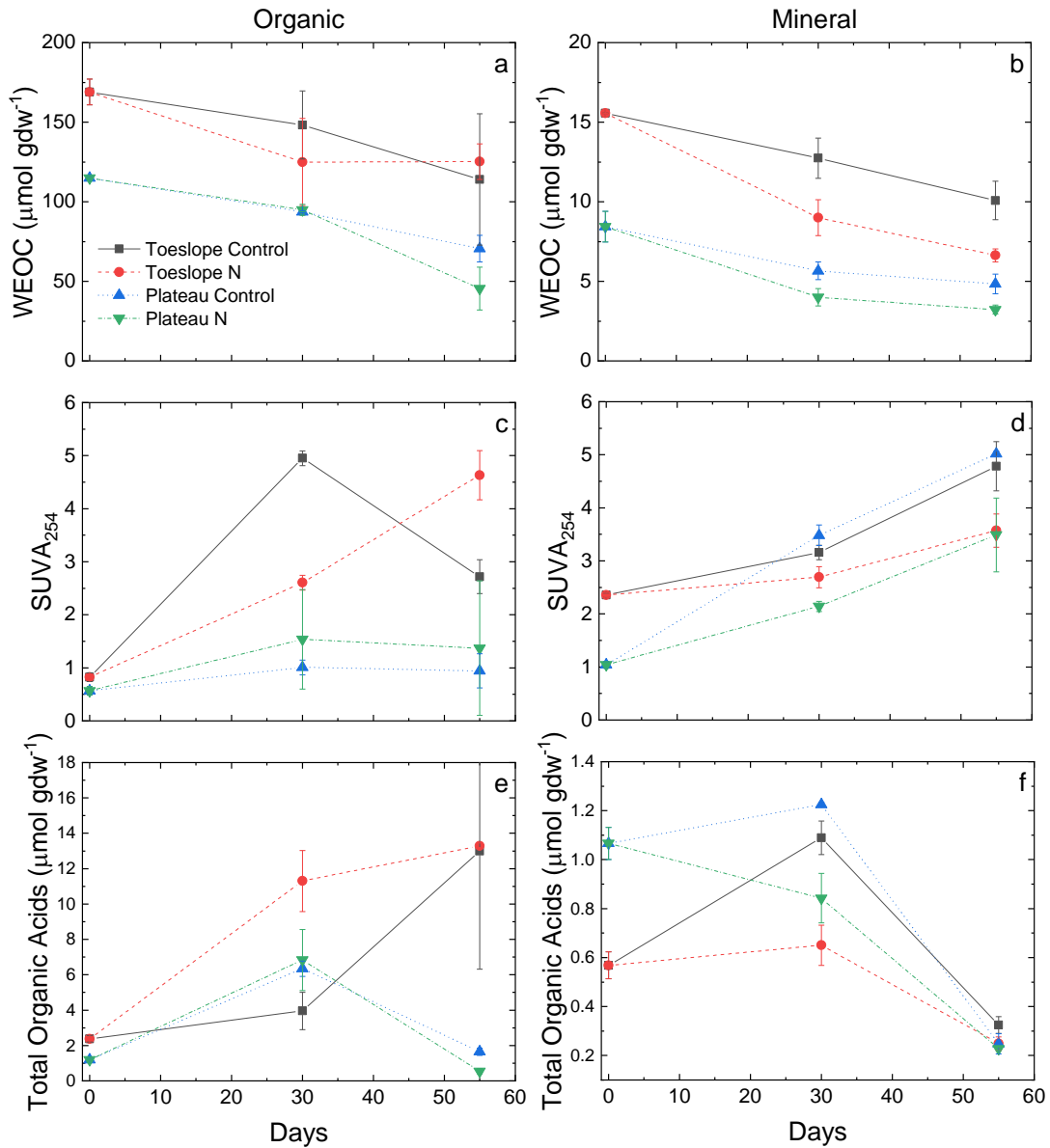
309 organic C was greater than the solubilization of solid-phase SOC. N addition significantly

310 increased the loss of WEOC after 55 days in all soils except for the toeslope organic soil.

311 SUVA₂₅₄ in the WEOC was slightly higher in the toeslope than the plateau organic soils at the
312 beginning of the experiment (0.82 and 0.57, respectively; $p = 0.014$), indicating higher
313 aromaticity. SUVA₂₅₄ increased significantly during incubation in all soils except for the organic
314 plateau (Fig. 3c). In the mineral soils, the SUVA₂₅₄ of the WEOC was higher than in the organic
315 soils (2.35 and 1.04 in the toeslope and plateau, respectively; Fig. 3d; $p = 0.014$ and 0.019,
316 respectively). N addition resulted in a smaller increase of SUVA₂₅₄ in the mineral soil control
317 incubations ($p < 0.001$), but not in the organic soils of both sites.

318 This pattern was also observed in the concentrations of low-molecular weight organic
319 acids, primarily formate, acetate, and propionate. Concentrations were higher in the organic soils
320 of the toeslope than the plateau (Fig. 3e). Concentrations in the toeslope organic soil increased
321 throughout the incubation, indicating the production of organic acids via fermentation exceeded
322 their consumption. In the plateau organic soil, concentrations increased from 0 to 30 days, but
323 then declined to near the initial concentration after 55 days. Both mineral soils exhibited a net
324 decline in organic acid concentrations by the end of the experiment (Fig. 3f). N addition appeared
325 to have little effect on the organic acid concentrations, and the final concentration was
326 significantly different only in the plateau organic soils (1.65 ± 0.20 and $0.55 \pm 0.16 \mu\text{mol gdw}^{-1}$
327 for control and +N treatments, respectively).

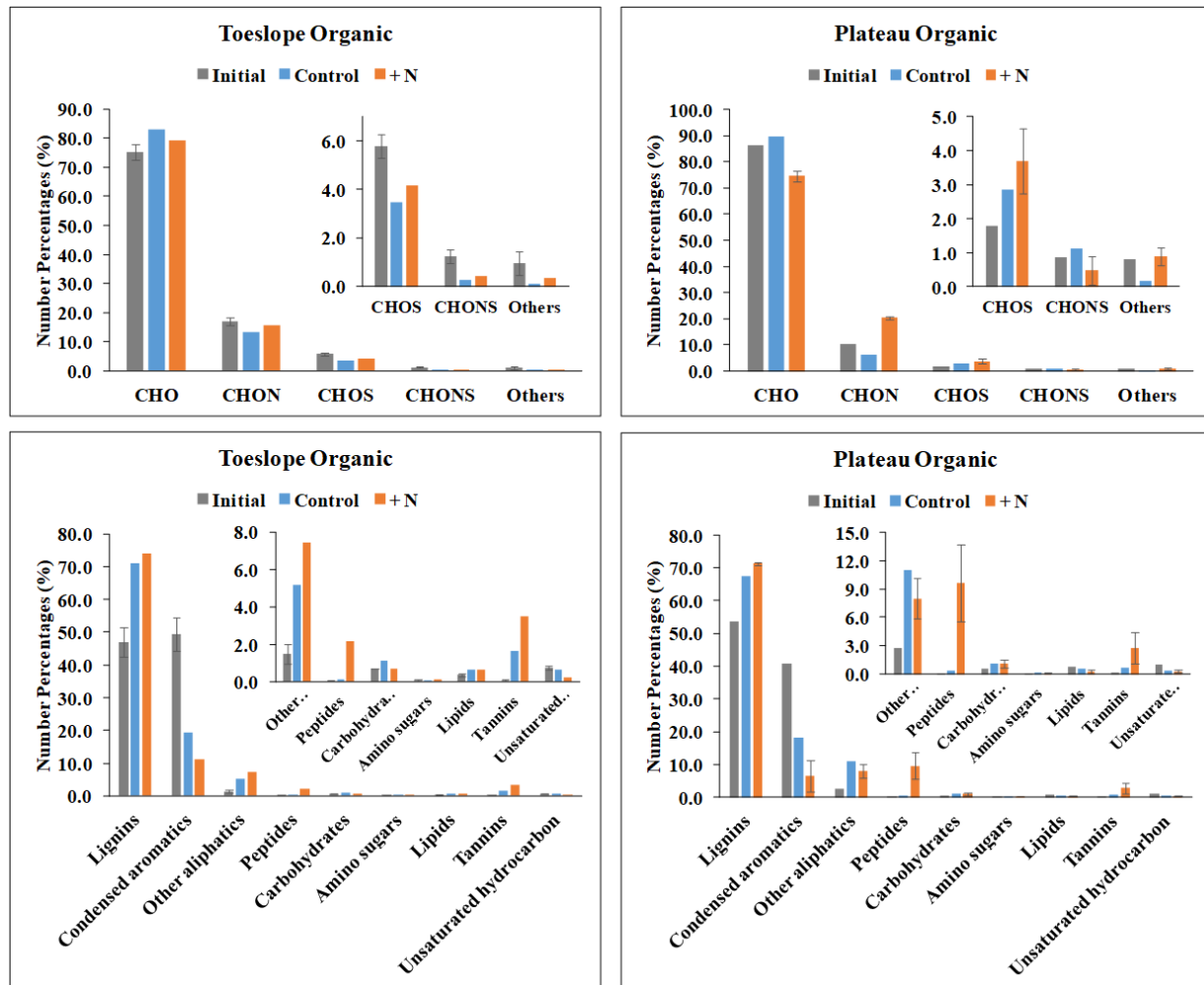
328



329

330 **Figure 3.** Water-extractable organic C (WEOC; a,b), specific ultraviolet absorbance at 254 nm
 331 (SUVA₂₅₄; c,d), and total extractable organic acids (sum of formate, acetate, propionate, and
 332 butyrate; e,f) in the initial soils and after 30 and 55 days of incubation. Symbols indicate the
 333 mean of three replicates and error bars indicate one standard deviation.

334



335

336 **Figure 4.** Relative abundance of molecular formulas from FTICR-MS analysis of the WEOC of
 337 the organic soils. Error bars indicate the deviation in results between sets of experimental
 338 replicates performed for selected samples.

339

340 FTICR-MS analysis of the WEOC indicated that formulas corresponding to lignin and
 341 condensed aromatic compounds were predominant in all porewater DOC samples (Fig. 4; Table
 342 S1). The number of lignin formulas increased in relative abundance during incubation, while
 343 condensed aromatics declined. The abundance of N-containing (CHON) and peptide formulas
 344 and their response to N addition varied by site. Between the organic soils, CHON formulas were
 345 more abundant in the toeslope than the plateau soils (16.9% and 10.4% of all formulas,

346 respectively; Fig. 4). Following N addition, the abundance of CHON formulas increased to
347 20.4% in the plateau soil, indicating incorporation of the added N into organic compounds, but
348 did not change in the toeslope soil. Peptide formulas also increased in abundance from <1% to
349 9.7% in the plateau N-addition incubation, but only increased to 2% in the toeslope soil
350 incubations.

351

352 3.5 Ion concentrations and pathways of anaerobic C decomposition

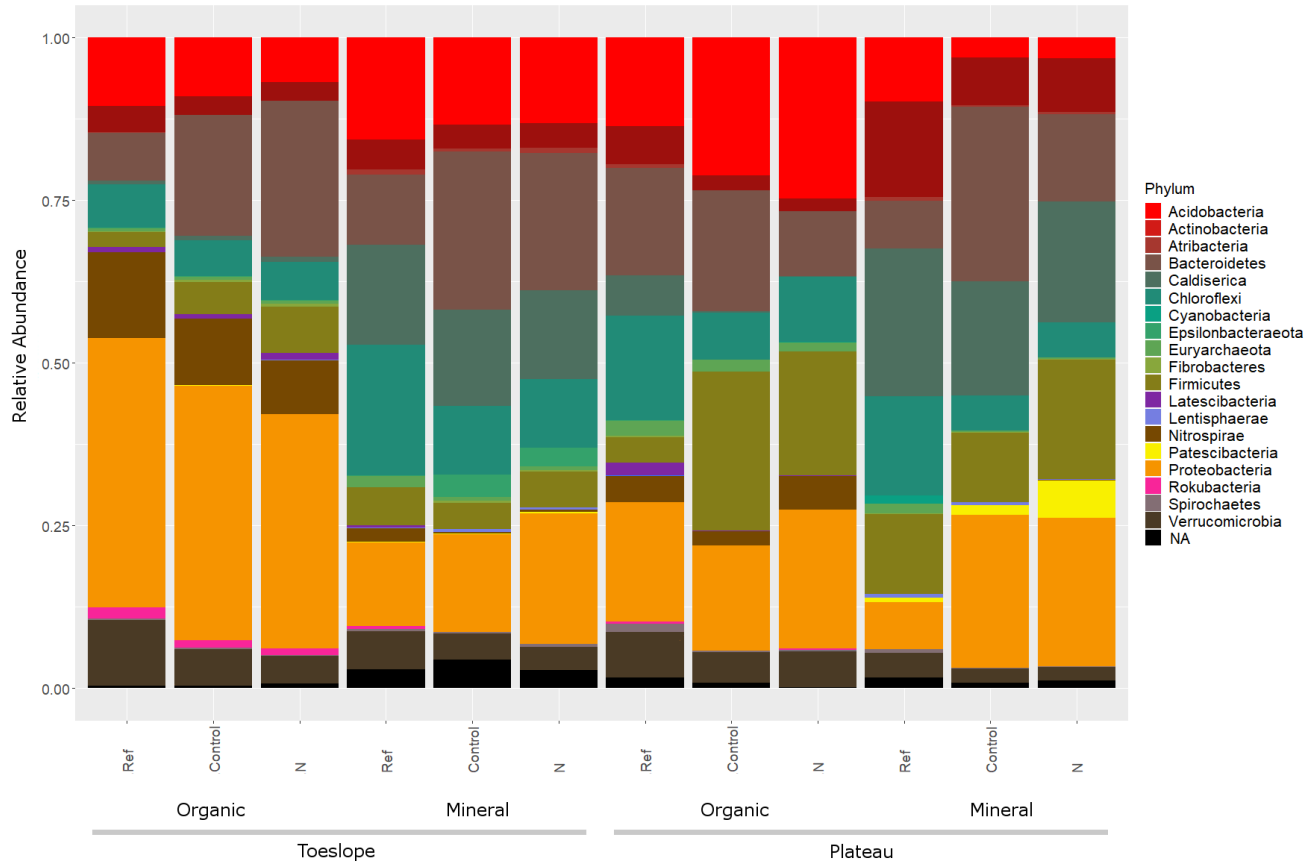
353 Changes of porewater ion concentrations during the incubations indicated a relatively
354 minor contribution of alternative electron acceptors to the total C mineralization. SO_4^{2-}
355 concentrations in the toeslope soils declined by 0.02-0.12 $\mu\text{mol gdw}^{-1}$ (Fig. S2), indicating that
356 SO_4^{2-} reduction accounted for <1% of the total C mineralization. In the plateau soils, SO_4^{2-}
357 concentrations increased slightly during incubation, and SO_4^{2-} reduction was not detectable.
358 Denitrification was also minimal, as NO_3^- declined by <0.07 $\mu\text{mol gdw}^{-1}$, consistent with low
359 initial NO_3^- concentrations (data not shown). Reduction of Fe(III) was detectable in all soils
360 except for the plateau mineral soil, as measured by increasing Fe(II) concentrations in the
361 porewater (Fig. S2). The cumulative increase in extractable Fe(II) ranged from 0.4 to 1.4 μmol
362 gdw^{-1} in the control treatments and 0 to 2.9 $\mu\text{mol gdw}^{-1}$ in the +N treatments, which were not
363 significantly different for any soil. However, Fe(III) reduction accounted for a small fraction of
364 C mineralization in all soils (<2%).

365

366 3.6 Microbial community composition

367 Microbial communities of toeslope and plateau soils were significantly different from
368 each other ($p = 0.005$) (Fig. S3). We also observed a strong effect ($p = 0.001$) where organic and

369 mineral soils in each location clustered separately indicating significant differences in each soil
370 compartment. *Proteobacteria*, *Bacteroides*, *Acidobacteria*, and *Chloroflexi* were abundant in all
371 soils (Fig. 5). *Caldiserica* were more abundant in the mineral soils than the organic soils.
372 Concentrations of WEOC ($p = 0.001$), propionate ($p = 0.001$), acetate ($p = 0.001$) and Fe(II) ($p =$
373 0.001) were significantly correlated with microbial community structure, especially in plateau
374 soils (Fig. S3). Soil pH overall showed a smaller correlation ($p = 0.006$) to the microbial
375 community structure. The effect of nitrogen addition on the microbial community was nuanced.
376 All soils clustered mainly based on their horizons ($p = 0.001$) where impact of nitrogen addition
377 was nested within each horizon ($p = 0.001$) and by itself was not a significant effect ($p = 0.881$).
378 Nitrogen addition effect was mainly observed as changes in microbial composition in
379 toeslope soils where *Firmicutes* significantly increased in both organic ($p = 0.035$) and mineral
380 ($p = 0.001$) soils with nitrogen addition (Fig. 5). Upon further analysis, we determined that
381 relative abundance of genus *Saccharofermentans* increased both in organic ($p = 0.025$) and
382 mineral ($p = 0.004$) soils in response to nitrogen addition (Fig. S5 and S6). Additionally, in
383 nitrogen-added mineral soils we detected significant increase in genus *Desulfosporosinus* ($p =$
384 0.045). In organic horizons of toeslope soils *Bacteroides* ($p = 0.008$) and *Proteobacteria* ($p =$
385 0.039) also increased in their relative abundance but remained unchanged in mineral soils (Fig.
386 5). Plateau soils responded differently to nitrogen addition than toeslope soils where the largest
387 and most significant change observed was the decrease in *Bacteroidetes* both in organic ($p =$
388 0.010) and mineral ($p < 0.001$) soils (Fig. 5). In both locations Archaeal populations was
389 dominated by methanogenic archaea of *Methanoflorentaceae* (former Rice Cluster II) (Adam et
390 al., 2017) (Fig. S8) which remained unchanged after nitrogen addition.



391

392 **Figure 5.** Relative abundance of microbial phyla extracted from the soils before and after
 393 incubation. NA: not assigned to a known phylum.

394

395 4 Discussion

396 4.1 Effects of topography on rates of SOM decomposition

397 Higher exchangeable aluminum and organic acid concentrations reduce the pH in the peat
 398 plateau soil compared to toeslope soils. Preliminary speciation calculations indicate that most of
 399 the aluminum, iron and alkaline earth metal ions in these pore waters are complexed by DOC.
 400 Therefore, the cation exchange capacities of DOC and SOM provide an important pH buffer to
 401 the soils. Similar precipitation-fed wetlands with no mineral inputs are often acidic due to the
 402 accumulation of organic acids resulting from fermentation (Gorham & Janssens, 1992). Synoptic
 403 sampling and analysis of the soil pore waters over three years have indicated that the soils from

404 the plateau have sodium bicarbonate-type pore waters, while the toeslope soil pore waters have a
405 calcium-magnesium bicarbonate chemistry with a lower ionic strength. These differences in pH
406 and geochemical environment are consistent with advanced mineral weathering and high cation
407 exchange capacity of peat in the plateau. At the base of the hillslope, however, runoff containing
408 leached alkaline earth metals floods tussock graminoid tundra. Therefore, the difference in pH
409 between the sites is associated with hillslope position, vegetation, and geomorphology.

410 Overall, our results show that both CO₂ and CH₄ production were higher in the organic
411 toeslope soils from the base of the hillslope than in the organic soils from the peat plateau. This
412 is likely in part due to the higher pH in the toeslope soils, which is a key control on anaerobic
413 SOM decomposition. Empirical estimates of the pH optimum for methanogenesis range from 6.2
414 to 7.5 (Cao et al., 1995; Meng et al., 2012; Tang et al., 2016). Observations of CO₂ and CH₄
415 emission also vary along natural pH gradients in peatlands (Moore & Knowles, 1990; Zalman et
416 al., 2018), and laboratory incubations show that buffering soils at a higher pH increases
417 production of both gasses, especially CH₄ (Dunfield et al., 1993; Valentine et al., 1994; Ye et al.,
418 2012). This is consistent with our observations of higher rates of CO₂ and CH₄ production in the
419 circumneutral toeslope soils. However, we observed that the hillslope position affected CO₂
420 much more than CH₄ production, resulting in lower CO₂:CH₄ ratios in the plateau soils than at
421 the base of the hillslope. This result contrasts with observations that methanogenesis is more
422 sensitive to pH than other pathways of anaerobic C mineralization, and suggests that other
423 hillslope differences such as differences in DOC concentration and composition also contribute
424 to the differences in greenhouse gas production.

425 Porewater DOC represents the fraction of C directly available to soil microorganisms,
426 and as such is the most important in shaping SOC decomposition dynamics (Chen et al., 2018;

427 Yang et al., 2016). For example, radiocarbon measurements of CH₄ in peatlands reflect the
428 young age of the DOC pool rather than the old age of the much larger SOC pool (Chanton et al.,
429 1995, 2008). Accordingly, some biogeochemical models estimate methanogenesis in part as a
430 function of DOC concentration (Cao et al., 1995, 1998; Tian et al., 2010; Xu & Tian, 2012).
431 WEOC represented a small fraction of the total SOC in both soils (0.33 and 0.24% in the organic
432 soils of the toeslope and plateau, respectively), but the concentrations were higher in the toeslope
433 soils. The higher concentrations of WEOC indicate a larger pool of potentially fermentable
434 substrates and likely contributes to the higher CO₂ and CH₄ production from these soils.

435 The patterns of WEOC concentrations during the incubations also suggest limitation of
436 labile C in the plateau soils. There was a net loss of WEOC during all incubations, indicating that
437 the degradation of DOC by microorganisms (or other uptake/immobilization) exceeded the
438 production of new DOC through the solubilization of solid-phase SOC. Consistent with previous
439 studies (Chen et al., 2018; Yang et al., 2016), the degradation of DOC was selective, as SUVA₂₅₄
440 values increased during the incubation. High SUVA₂₅₄ values are correlated with the abundance
441 of aromatic DOC and are associated with lower CH₄ production (D'Andrilli et al., 2010;
442 Hodgkins et al., 2016). The inhibitory effect of highly aromatic DOC on C mineralization could
443 be higher in these anaerobic incubations due to the low activity of phenol oxidase in the absence
444 of oxygen (Freeman et al., 2004; Pind et al., 1994). Therefore, our results indicate selective
445 decomposition of the bioavailable and easily fermentable DOC pool, and accumulation of the
446 aromatic fraction. This effect was more pronounced in the plateau soils where initial DOC
447 concentrations were lower. The depletion of easily fermentable C likely contributes to the lower
448 CO₂ and CH₄ production in the organic soils.

449 Limitation of bioavailable DOC was also apparent in the concentrations of low molecular
450 weight organic acids, the immediate substrates for methanogenesis as well as Fe(III) and SO_4^{2-}
451 reduction in these soils (Bethke et al., 2011). Models (Tang et al., 2016; Zheng et al., 2019a),
452 observations (Christensen et al., 2003; Valentine et al., 1994), and experiments (Herndon et al.,
453 2015; Hershey et al., 2014) indicate that the availability of these substrates limits rates of
454 methanogenesis and anaerobic C mineralization. The increasing organic acid concentrations in
455 the organic toeslope soils indicated that their production via fermentation exceeded their
456 utilization, and they were therefore not limiting for anaerobic respiration. This was supported by
457 the stable microbial community structure in soils with prevalence of carbohydrate-fermenting
458 populations such as *Firmicutes* and *Bacteroidetes*. In contrast, the pattern of organic acid
459 concentrations and microbial community composition in the mineral horizons suggests substrate
460 limitation of respiration. In the toeslope organic soil, increases in the carbohydrate-fermenting
461 genus *Saccharofermentans* and *Desulfosporosinus*, which includes bacteria capable of anaerobic
462 respiration using sulfate, Fe (III) or fumarate as electron acceptors, suggests close coupling of
463 organic acid fermentation and anaerobic respiration (Chen, 2017; Nixon et al., 2017). In plateau
464 mineral soil horizons, observed increases in Group I clostridia (*Clostridium sensu stricto*) (Gupta
465 & Gao, 2009) signals the emergence of fermentative pathways leading to alcohol, butyrate,
466 acetate and hydrogen production. In both locations and soil horizons relative abundance of the
467 dominant methanogenic lineage *Methanoflorentaceae* (former Rice Cluster II) showed no
468 significant change with incubation, yet we observed different CH_4 production rates. The
469 hydrogenotrophic methanogen candidatus *Methanoflorens stordalenmirensis* was identified as
470 the predominant methanogen in a northern Sweden permafrost thaw site (Mondav et al., 2014).
471 The strong correlation of WEOC and organic acid concentrations with the overall microbial

472 community composition (Fig. S3) provides other lines of evidence that substrate availability was
473 a key control on microbial growth. Therefore, we conclude that continued bioavailability of
474 WEOC (Fig. 3) in the toeslope supported a higher rate of fermentation, in turn fueling higher
475 rates of CO₂ and CH₄ production.

476

477 4.2 Greater microbial N limitation in the plateau soils

478 Several lines of evidence indicate that the plateau soils were more N-limited than the
479 toeslope soils, especially in the organic soil. First, the concentration of extractable inorganic N
480 (NO₃⁻+NH₄⁺) was higher in the organic soils of the toeslope than the plateau. Second, extractable
481 inorganic N increased during the incubation of the toeslope organic control soils, indicating net
482 N mineralization. This is consistent with previous observations that net N mineralization is
483 generally higher in soils in lower topographic positions (Giblin et al., 1991; Nadelhoffer et al.,
484 1991). In contrast to the toeslope organic soil, both plateau soils exhibited declining inorganic N
485 concentrations during incubation, indicating either net N immobilization or gaseous N losses.
486 This observation is consistent with greater N availability in the toeslope soils. The increase in
487 CHON and peptide formulas following N addition in the plateau but not the toeslope organic
488 soils by FTICR-MS analysis also demonstrates that the added N was assimilated to a greater
489 degree in the plateau soils, consistent with greater microbial N limitation. Finally, N addition
490 increased CO₂ production in the organic plateau soils but not the toeslope soils, further
491 demonstrating that SOM decomposition was N-limited in the former but not the latter.

492 Although we do not have direct evidence of the sources of N to the toeslope soils, these
493 patterns are consistent with leaching and downslope transport of inorganic and labile organic N
494 down the hillslope. The differences in pH, ion composition, and alkali-to-alkaline earth metal

495 ratio of the porewater demonstrate distinct sources of water inputs, indicating the water in the
496 toeslope soils is derived from hillslope runoff. Previous studies have demonstrated that nutrients
497 (including N) are transported downslope and accumulate in low-lying areas (Stewart et al.,
498 2014). Our results extend these findings to tundra landscapes and demonstrate that they cause
499 associated differences in anaerobic SOM decomposition. The hillslope gradient in decomposition
500 is similar to the hydrological fen-bog gradient in peatlands, in which wetlands with higher pH
501 and nutrient availability are associated with higher rates of anaerobic SOM decomposition,
502 especially CH₄ production (Keller et al., 2006; Thormann et al., 1999; Ye et al., 2012).

503 Our experiments utilized cores collected in early June, before the Arctic growing season.
504 N limitation in tundra soils is observed to be highest at the peak of the growing season, when
505 plants and microorganisms are competing for available N (Melle et al., 2015). These microcosm
506 incubation experiments are therefore conservative estimates of the potential N limitation of
507 SOM decomposition; the lack of effect of N addition on CO₂ production in the toeslope soils
508 does not preclude N limitation during the summer, as has been observed previously (Philben et
509 al., 2019). However, our results are consistent with relatively greater N limitation in the plateau
510 soils compared to the toeslope.

511 In contrast to the organic soils, there was no evidence that N availability in the mineral
512 soils differed between the plateau and the toeslope. There was no difference in initial extractable
513 N content. No net N mineralization was observed in the toeslope soils, and N addition did not
514 significantly increase CO₂ production. This indicates that the apparent microbial N limitation
515 was limited to the organic plateau soil. Mineral soils could therefore experience a smaller
516 increase in CO₂ production in response to increased N availability.

517 While N addition stimulated CO₂ production in the organic plateau soil, it consistently
518 decreased CH₄ production in all but one soil (the plateau mineral soil). This likely results from
519 suppression of methanogenesis due to reduced pH. The pH optimum for methanogenesis is
520 between 6 and 7, and the slope of the response function appears to be steeper than that of CO₂
521 production due to the specificity of the microbes and enzymes involved (Ye et al., 2012). The pH
522 of the KCl extracts following incubation was consistently lower in the microcosms with added
523 NH₄Cl compared to the control microcosms. This was in part due to the weakly acidic nature of
524 the NH₄Cl solution (pH ~5.7), but also likely due to the effects of increased proton production
525 via fermentation, especially in the plateau soils. The lower pH in the N-fertilized treatments
526 could result in reduced CH₄ production despite other indicators of microbial N limitation,
527 emphasizing the complex feedbacks regulating CH₄ production.

528 **5 Conclusions**

529 We observed major differences in the rates of greenhouse gas production in two wetland
530 areas within the same watershed. Despite surface similarities between the wetland areas, the
531 toeslope organic soil produced significantly more CO₂ and CH₄ than the plateau soil due to
532 higher availability of labile DOC and higher pH than the plateau soils during anaerobic
533 incubation. Our results also indicate that inorganic N concentrations were lower and soil C
534 decomposition was more N-limited in the plateau soils than the toeslope soils, which exhibited
535 net N mineralization while the plateau soils had net N immobilization. Examination of the
536 changes in porewater geochemistry, soil microbial community and response to N addition
537 indicate that the differences are due to a combination of (1) higher pH due to leaching of mineral
538 weathering products from the hillslope; (2) higher N availability for microorganisms; and (3)
539 higher availability of fermentable DOC, which provided an ample supply of labile organic

540 substrates throughout the incubations in the toeslope soils. These results demonstrate that
541 topographic position, geochemical environment, and hydrologic flow are important
542 considerations to predict the fate of thawing permafrost.

543 **Acknowledgments and data availability**

544 The authors declare no financial conflicts of interest. All data supporting the conclusions of
545 this work can be found on the NGEE-Arctic Data Portal (<https://ngee-arctic.ornl.gov/data>).

546 We thank Xiangping Yin for ICP-MS analyses of samples and technical support in
547 laboratory. Xujun Liang and Jianqiu Zheng assisted constructing the soil microcosms. The Next
548 Generation Ecosystem Experiments (NGEE-Arctic) project is supported by the Office of
549 Biological and Environmental Research in the Department of Energy (DOE) Office of Science.
550 Oak Ridge National Laboratory is managed by UT-Battelle LLC for DOE under contract DE-
551 AC05-00OR22725.

552 **References**

- 553 Adam, P. S., Borrel, G., Brochier-Armanet, C., & Gribaldo, S. (2017). The growing tree of
554 Archaea: new perspectives on their diversity, evolution and ecology. *The ISME Journal*,
555 11(11), 2407–2425. <https://doi.org/10.1038/ismej.2017.122>
- 556 Anderson, M. J., & Walsh, D. C. I. (2013). PERMANOVA, ANOSIM, and the Mantel test in the
557 face of heterogeneous dispersions: What null hypothesis are you testing? *Ecological*
558 *Monographs*, 83(4), 557–574. <https://doi.org/10.1890/12-2010.1>
- 559 Bates, D., Maechler, M., Bolker, B., & Walker, S. (2014). *lme4: Linear mixed-effects models*
560 *using Eigen and S4*. *R package version 1.1-7*.
- 561 Bayley, S. E., Thormann, M. N., & Szumigalski, A. R. (2005). Nitrogen mineralization and
562 decomposition in western boreal bog and fen peat. *Ecoscience*, 12(4), 455–465.
563 <https://doi.org/10.2980/i1195-6860-12-4-455.1>
- 564 Bethke, C. M., Sanford, R. A., Kirk, M. F., Jin, Q., & Flynn, T. M. (2011). The thermodynamic
565 ladder in geomicrobiology. *American Journal of Science*, 311(3), 183–210.
566 <https://doi.org/10.2475/03.2011.01>
- 567 Bokulich, N. A., Subramanian, S., Faith, J. J., Gevers, D., Gordon, J. I., Knight, R., et al. (2013).
568 Quality-filtering vastly improves diversity estimates from Illumina amplicon sequencing.
569 *Nature Methods*, 10(1), 57–59. <https://doi.org/10.1038/nmeth.2276>

- 570 Bray, J. R., & Curtis, J. T. (1957). An Ordination of the Upland Forest Communities of Southern
571 Wisconsin. *Ecological Monographs*, 27(4), 325–349. <https://doi.org/10.2307/1942268>
- 572 Bring, A., Fedorova, I., Dibike, Y., Hinzman, L., Mård, J., Mernild, S. H., et al. (2016). Arctic
573 terrestrial hydrology: A synthesis of processes, regional effects, and research challenges.
574 *Journal of Geophysical Research: Biogeosciences*, 121(3), 621–649.
575 <https://doi.org/10.1002/2015JG003131>
- 576 Burt, T. P., & Pinay, G. (2005). Linking hydrology and biogeochemistry in complex landscapes.
577 *Progress in Physical Geography: Earth and Environment*, 29(3), 297–316.
578 <https://doi.org/10.1191/0309133305pp450ra>
- 579 Cao, M., Dent, J. B., & Heal, O. W. (1995). Modeling methane emissions from rice paddies.
580 *Global Biogeochemical Cycles*, 9(2), 183–195. <https://doi.org/10.1029/94GB03231>
- 581 Cao, M., Gregson, K., & Marshall, S. (1998). Global methane emission from wetlands and its
582 sensitivity to climate change. *Atmospheric Environment*, 32(19), 3293–3299.
583 [https://doi.org/10.1016/S1352-2310\(98\)00105-8](https://doi.org/10.1016/S1352-2310(98)00105-8)
- 584 Caporaso, J. G., Kuczynski, J., Stombaugh, J., Bittinger, K., Bushman, F. D., Costello, E. K., et
585 al. (2010). QIIME allows analysis of high-throughput community sequencing data.
586 *Nature Methods*, 7(5), 335. <https://doi.org/10.1038/nmeth.f.303>
- 587 Chanton, J. P., Bauer, J. E., Glaser, P. A., Siegel, D. I., Kelley, C. A., Tyler, S. C., et al. (1995).
588 Radiocarbon evidence for the substrates supporting methane formation within northern
589 Minnesota peatlands. *Geochimica et Cosmochimica Acta*, 59(17), 3663–3668.
590 [https://doi.org/10.1016/0016-7037\(95\)00240-Z](https://doi.org/10.1016/0016-7037(95)00240-Z)
- 591 Chanton, J. P., Glaser, P. H., Chasar, L. S., Burdige, D. J., Hines, M. E., Siegel, D. I., et al.
592 (2008). Radiocarbon evidence for the importance of surface vegetation on fermentation
593 and methanogenesis in contrasting types of boreal peatlands. *Global Biogeochemical*
594 *Cycles*, 22(4), GB4022. <https://doi.org/10.1029/2008GB003274>
- 595 Chen, H., Yang, Z., Chu, R. K., Tolic, N., Liang, L., Graham, D. E., et al. (2018). Molecular
596 Insights into Arctic Soil Organic Matter Degradation under Warming. *Environmental*
597 *Science & Technology*, 52(8), 4555–4564. <https://doi.org/10.1021/acs.est.7b05469>
- 598 Chen, S. (2017). Saccharofermentans. In *Bergey's Manual of Systematics of Archaea and*
599 *Bacteria* (pp. 1–5). American Cancer Society.
600 <https://doi.org/10.1002/9781118960608.gbm01450>
- 601 Christensen, T. R., Ekberg, A., Ström, L., Mastepanov, M., Panikov, N., Öquist, M., et al.
602 (2003). Factors controlling large scale variations in methane emissions from wetlands.
603 *Geophysical Research Letters*, 30(7), 1414. <https://doi.org/10.1029/2002GL016848>
- 604 Creed, I. F., Trick, C. G., Band, L. E., & Morrison, I. K. (2002). Characterizing the Spatial
605 Pattern of Soil Carbon and Nitrogen Pools in the Turkey Lakes Watershed: A
606 Comparison of Regression Techniques. *Water, Air and Soil Pollution: Focus*, 2(1), 81–
607 102. <https://doi.org/10.1023/A:1015886308016>
- 608 D'Andrilli, J., Chanton, J. P., Glaser, P. H., & Cooper, W. T. (2010). Characterization of
609 dissolved organic matter in northern peatland soil porewaters by ultra high resolution

- 610 mass spectrometry. *Organic Geochemistry*, 41(8), 791–799.
611 <https://doi.org/10.1016/j.orggeochem.2010.05.009>
- 612 Dittmar, T., Koch, B., Hertkorn, N., & Kattner, G. (2008). A simple and efficient method for the
613 solid-phase extraction of dissolved organic matter (SPE-DOM) from seawater.
614 *Limnology and Oceanography: Methods*, 6(6), 230–235.
- 615 Dunfield, P., Knowles, R., Dumont, R., & Moore, T. R. (1993). Methane production and
616 consumption in temperate and subarctic peat soils: Response to temperature and pH. *Soil*
617 *Biology and Biochemistry*, 25(3), 321–326. [https://doi.org/10.1016/0038-0717\(93\)90130-](https://doi.org/10.1016/0038-0717(93)90130-4)
618 4
- 619 Edgar, R. C. (2013). UPARSE: highly accurate OTU sequences from microbial amplicon reads.
620 *Nature Methods*, 10(10), 996–998. <https://doi.org/10.1038/nmeth.2604>
- 621 Fan, Y., Clark, M., Lawrence, D. M., Swenson, S., Band, L. E., Brantley, S. L., et al. (2019).
622 Hillslope hydrology in global change research and Earth system modeling. *Water*
623 *Resources Research*, 55(2), 1737–1772. <https://doi.org/10.1029/2018WR023903>
- 624 Freeman, C., Ostle, N. J., Fenner, N., & Kang, H. (2004). A regulatory role for phenol oxidase
625 during decomposition in peatlands. *Soil Biology and Biochemistry*, 36(10), 1663–1667.
626 <https://doi.org/10.1016/j.soilbio.2004.07.012>
- 627 Giblin, A. E., Nadelhoffer, K. J., Shaver, G. R., Laundre, J. A., & McKerrow, A. J. (1991).
628 Biogeochemical Diversity Along a Riverside Toposequence in Arctic Alaska. *Ecological*
629 *Monographs*, 61(4), 415–435. <https://doi.org/10.2307/2937049>
- 630 Gorham, E., & Janssens, J. A. (1992). Concepts of fen and bog re-examined in relation to
631 bryophyte cover and the acidity of surface waters. *Acta Societatis Botanicorum Poloniae*,
632 61(1), 8. <https://doi.org/10.5586/asbp.1992.001>
- 633 Gupta, R. S., & Gao, B. (2009). Phylogenomic analyses of clostridia and identification of novel
634 protein signatures that are specific to the genus *Clostridium sensu stricto* (cluster I).
635 *International Journal of Systematic and Evolutionary Microbiology*, 59(2), 285–294.
636 <https://doi.org/10.1099/ijs.0.001792-0>
- 637 Hall, G. F., & Olson, C. G. (1991). Predicting variability of soils from landscape models. *Spatial*
638 *Variabilities of Soils and Landforms*, 9–24.
- 639 Herndon, E. M., Mann, B. F., Roy Chowdhury, T., Yang, Z., Wulfschleger, S. D., Graham, D., et
640 al. (2015). Pathways of anaerobic organic matter decomposition in tundra soils from
641 Barrow, Alaska. *Journal of Geophysical Research: Biogeosciences*, 120(11), 2345–2359.
642 <https://doi.org/10.1002/2015JG003147>
- 643 Hershey, A. E., Northington, R. M., & Whalen, S. C. (2014). Substrate limitation of sediment
644 methane flux, methane oxidation and use of stable isotopes for assessing methanogenesis
645 pathways in a small arctic lake. *Biogeochemistry*, 117(2–3), 325–336.
646 <https://doi.org/10.1007/s10533-013-9864-y>
- 647 Hodgkins, S. B., Tfaily, M. M., Podgorski, D. C., McCalley, C. K., Saleska, S. R., Crill, P. M., et
648 al. (2016). Elemental composition and optical properties reveal changes in dissolved
649 organic matter along a permafrost thaw chronosequence in a subarctic peatland.

- 650 Geochimica et Cosmochimica Acta, 187, 123–140.
651 <https://doi.org/10.1016/j.gca.2016.05.015>
- 652 Hornberger, G. M., Bencala, K. E., & McKnight, D. M. (1994). Hydrological controls on
653 dissolved organic carbon during snowmelt in the Snake River near Montezuma,
654 Colorado. *Biogeochemistry*, 25(3), 147–165. <https://doi.org/10.1007/BF00024390>
- 655 Hugelius, G., Strauss, J., Zubrzycki, S., Harden, J. W., Schuur, E. A. G., Ping, C.-L., et al.
656 (2014). Estimated stocks of circumpolar permafrost carbon with quantified uncertainty
657 ranges and identified data gaps. *Biogeosciences*, 11(23). [https://doi.org/10.5194/bg-11-](https://doi.org/10.5194/bg-11-6573-2014)
658 [6573-2014](https://doi.org/10.5194/bg-11-6573-2014)
- 659 Jafarov, E. E., Coon, E. T., Harp, D. R., Wilson, C. J., Painter, S. L., Atchley, A. L., &
660 Romanovsky, V. E. (2018). Modeling the role of preferential snow accumulation in
661 through talik development and hillslope groundwater flow in a transitional permafrost
662 landscape. *Environmental Research Letters*, 13(10), 105006.
663 <https://doi.org/10.1088/1748-9326/aadd30>
- 664 Keller, J. K., Bauers, A. K., Bridgham, S. D., Kellogg, L. E., & Iversen, C. M. (2006). Nutrient
665 control of microbial carbon cycling along an ombrotrophic-minerotrophic peatland
666 gradient. *Journal of Geophysical Research: Biogeosciences*, 111(G3), G03006.
667 <https://doi.org/10.1029/2005JG000152>
- 668 Koch, B. P., & Dittmar, T. (2006). From mass to structure: An aromaticity index for high-
669 resolution mass data of natural organic matter. *Rapid Communications in Mass*
670 *Spectrometry*, 20(5), 926–932. <https://doi.org/10.1002/rcm.2386>
- 671 Koch, J. C., Gurney, K., & Wipfli, M. S. (2014). Morphology-dependent water budgets and
672 nutrient fluxes in Arctic thaw ponds. *Permafrost and Periglacial Processes*, 25(2), 79–93.
673 <https://doi.org/10.1002/ppp.1804>
- 674 Lev, A., & King, R. H. (1999). Spatial variation of soil development in a high arctic soil
675 landscape: Truelove Lowland, Devon Island, Nunavut, Canada. *Permafrost and*
676 *Periglacial Processes*, 10(3), 289–307. [https://doi.org/10.1002/\(SICI\)1099-](https://doi.org/10.1002/(SICI)1099-1530(199907/09)10:3<289::AID-PPP319>3.0.CO;2-Z)
677 [1530\(199907/09\)10:3<289::AID-PPP319>3.0.CO;2-Z](https://doi.org/10.1002/(SICI)1099-1530(199907/09)10:3<289::AID-PPP319>3.0.CO;2-Z)
- 678 Liljedahl, A. K., Boike, J., Daanen, R. P., Fedorov, A. N., Frost, G. V., Grosse, G., et al. (2016).
679 Pan-Arctic ice-wedge degradation in warming permafrost and its influence on tundra
680 hydrology. *Nature Geoscience*, 9(4), 312–318. <https://doi.org/10.1038/ngeo2674>
- 681 Magoč, T., & Salzberg, S. L. (2011). FLASH: fast length adjustment of short reads to improve
682 genome assemblies. *Bioinformatics*, 27(21), 2957–2963.
683 <https://doi.org/10.1093/bioinformatics/btr507>
- 684 McMurdie, P. J., & Holmes, S. (2013). phyloseq: An R Package for Reproducible Interactive
685 Analysis and Graphics of Microbiome Census Data. *PLOS ONE*, 8(4), e61217.
686 <https://doi.org/10.1371/journal.pone.0061217>
- 687 Melle, C., Wallenstein, M., Darrouzet-Nardi, A., & Weintraub, M. N. (2015). Microbial activity
688 is not always limited by nitrogen in Arctic tundra soils. *Soil Biology and Biochemistry*,
689 90, 52–61. <https://doi.org/10.1016/j.soilbio.2015.07.023>

- 690 Meng, L., Hess, P. G. M., Mahowald, N. M., Yavitt, J. B., Riley, W. J., Subin, Z. M., et al.
691 (2012). Sensitivity of wetland methane emissions to model assumptions: application and
692 model testing against site observations. *Biogeosciences*, 9(7), 2793–2819.
693 <https://doi.org/10.5194/bg-9-2793-2012>
- 694 Metcalfe, D. B., Hermans, T. D., Ahlstrand, J., Becker, M., Berggren, M., Björk, R. G., et al.
695 (2018). Patchy field sampling biases understanding of climate change impacts across the
696 Arctic. *Nature Ecology & Evolution*, 2(9), 1443–1448. [https://doi.org/10.1038/s41559-](https://doi.org/10.1038/s41559-018-0612-5)
697 [018-0612-5](https://doi.org/10.1038/s41559-018-0612-5)
- 698 Milne, G. (1936). Normal erosion as a factor in soil profile development. *Nature*, 138(3491),
699 548–549.
- 700 Monday, R., Woodcroft, B. J., Kim, E.-H., McCalley, C. K., Hodgkins, S. B., Crill, P. M., et al.
701 (2014). Discovery of a novel methanogen prevalent in thawing permafrost. *Nature*
702 *Communications*, 5(1), 1–7. <https://doi.org/10.1038/ncomms4212>
- 703 Moore, I. D., Gessler, P. E., Nielsen, G. A. E., & Peterson, G. A. (1993). Soil attribute prediction
704 using terrain analysis. *Soil Science Society of America Journal*, 57(2), 443–452.
705 <https://doi.org/10.2136/sssaj1993.03615995005700020026x>
- 706 Moore, T. R., & Knowles, R. (1990). Methane emissions from fen, bog and swamp peatlands in
707 Quebec. *Biogeochemistry*, 11(1), 45–61. <https://doi.org/10.1007/BF00000851>
- 708 Nadelhoffer, K. J., Giblin, A. E., Shaver, G. R., & Laundre, J. A. (1991). Effects of temperature
709 and substrate quality on element mineralization in six arctic soils. *Ecology*, 72(1), 242–
710 253. <https://doi.org/10.2307/1938918>
- 711 Nixon, S. L., Telling, J. P., Wadham, J. L., & Cockell, C. S. (2017). Viable cold-tolerant iron-
712 reducing microorganisms in geographically diverse subglacial environments.
713 *Biogeosciences*, 14(6), 1445–1455. <https://doi.org/10.5194/bg-14-1445-2017>
- 714 Oksanen, J., Blanchet, F. G., Kindt, R., Legendre, P., Minchin, P. R., O’hara, R. B., et al. (2013).
715 Package ‘vegan.’ *Community Ecology Package, Version*, 2(9), 1–295.
- 716 Patil, I., Powell, C., Beasley, W., & Heck, D. (2019). ggstatsplot: major restructuring of the
717 entire package. Zenodo. <https://doi.org/10.5281/zenodo.3382322>
- 718 Philben, M., Zheng, J., Bill, M., Heikoop, J. M., Perkins, G., Yang, Z., et al. (2019). Stimulation
719 of anaerobic organic matter decomposition by subsurface organic N addition in tundra
720 soils. *Soil Biology and Biochemistry*, 130, 195–204.
721 <https://doi.org/10.1016/j.soilbio.2018.12.009>
- 722 Pind, A., Freeman, C., & Lock, M. A. (1994). Enzymic degradation of phenolic materials in
723 peatlands—measurement of phenol oxidase activity. *Plant and Soil*, 159(2), 227–231.
724 <https://doi.org/10.1007/BF00009285>
- 725 Price, M. N., Dehal, P. S., & Arkin, A. P. (2010). FastTree 2 – Approximately Maximum-
726 Likelihood Trees for Large Alignments. *PLOS ONE*, 5(3), e9490.
727 <https://doi.org/10.1371/journal.pone.0009490>
- 728 Quast, C., Pruesse, E., Yilmaz, P., Gerken, J., Schweer, T., Yarza, P., et al. (2013). The SILVA
729 ribosomal RNA gene database project: improved data processing and web-based tools.
730 *Nucleic Acids Research*, 41(D1), D590–D596. <https://doi.org/10.1093/nar/gks1219>

- 731 Roy Chowdhury, T., Herndon, E. M., Phelps, T. J., Elias, D. A., Gu, B., Liang, L., et al. (2015).
732 Stoichiometry and temperature sensitivity of methanogenesis and CO₂ production from
733 saturated polygonal tundra in Barrow, Alaska. *Global Change Biology*, 21(2), 722–737.
734 <https://doi.org/10.1111/gcb.12762>
- 735 Sander, R. (2015). Compilation of Henry's law constants (version 4.0) for water as solvent.
736 *Atmospheric Chemistry & Physics*, 15(8), 4399–4981. [https://doi.org/10.5194/acp-15-](https://doi.org/10.5194/acp-15-4399-2015)
737 [4399-2015](https://doi.org/10.5194/acp-15-4399-2015)
- 738 Schuur, E. A., McGuire, A. D., Schädel, C., Grosse, G., Harden, J. W., Hayes, D. J., et al.
739 (2015). Climate change and the permafrost carbon feedback. *Nature*, 520(7546), 171–
740 179. <https://doi.org/10.1038/nature14338>
- 741 Stewart, K. J., Grogan, P., Coxson, D. S., & Siciliano, S. D. (2014). Topography as a key factor
742 driving atmospheric nitrogen exchanges in arctic terrestrial ecosystems. *Soil Biology and*
743 *Biochemistry*, 70, 96–112. <https://doi.org/10.1016/j.soilbio.2013.12.005>
- 744 Stieglitz, M., Shaman, J., McNamara, J., Engel, V., Shanley, J., & Kling, G. W. (2003). An
745 approach to understanding hydrologic connectivity on the hillslope and the implications
746 for nutrient transport. *Global Biogeochemical Cycles*, 17(4), 1105.
747 <https://doi.org/10.1029/2003GB002041>
- 748 Tang, G., Zheng, J., Xu, X., Yang, Z., Graham, D. E., Gu, B., et al. (2016). Biogeochemical
749 modeling of CO₂ and CH₄ production in anoxic Arctic soil microcosms.
750 *Biogeosciences*, 13(17), 5021–5041. <https://doi.org/10.5194/bg-13-5021-2016>
- 751 Thormann, M. N., Szumigalski, A. R., & Bayley, S. E. (1999). Aboveground peat and carbon
752 accumulation potentials along a bog-fen-marsh wetland gradient in southern boreal
753 Alberta, Canada. *Wetlands*, 19(2), 305–317. <https://doi.org/10.1007/BF03161761>
- 754 Tian, H., Xu, X., Liu, M., Ren, W., Zhang, C., Chen, G., & Lu, C. (2010). Spatial and temporal
755 patterns of CH₄ and N₂O fluxes in terrestrial ecosystems of North America during
756 1979–2008: application of a global biogeochemistry model. *Biogeosciences*, 7(9), 2673–
757 2694. <https://doi.org/10.5194/bg-7-2673-2010>
- 758 Valentine, D. W., Holland, E. A., & Schimel, D. S. (1994). Ecosystem and physiological controls
759 over methane production in northern wetlands. *Journal of Geophysical Research:*
760 *Atmospheres*, 99(D1), 1563–1571. <https://doi.org/10.1029/93JD00391>
- 761 Wang, H. J., Shi, X. Z., Yu, D. S., Weindorf, D. C., Huang, B., Sun, W. X., et al. (2009). Factors
762 determining soil nutrient distribution in a small-scaled watershed in the purple soil region
763 of Sichuan Province, China. *Soil and Tillage Research*, 105(2), 300–306.
764 <https://doi.org/10.1016/j.still.2008.08.010>
- 765 Wang, Q., Garrity, G. M., Tiedje, J. M., & Cole, J. R. (2007). Naïve Bayesian Classifier for
766 Rapid Assignment of rRNA Sequences into the New Bacterial Taxonomy. *Applied and*
767 *Environmental Microbiology*, 73(16), 5261–5267. [https://doi.org/10.1128/AEM.00062-](https://doi.org/10.1128/AEM.00062-07)
768 [07](https://doi.org/10.1128/AEM.00062-07)
- 769 Weishaar, J. L., Aiken, G. R., Bergamaschi, B. A., Fram, M. S., Fujii, R., & Mopper, K. (2003).
770 Evaluation of specific ultraviolet absorbance as an indicator of the chemical composition
771 and reactivity of dissolved organic carbon. *Environmental Science & Technology*,
772 37(20), 4702–4708. <https://doi.org/10.1021/es030360x>

- 773 Xu, X., & Tian, H. (2012). Methane exchange between marshland and the atmosphere over
774 China during 1949–2008. *Global Biogeochemical Cycles*, 26(2), GB2006.
775 <https://doi.org/10.1029/2010GB003946>
- 776 Yang, Z., Wullschleger, S. D., Liang, L., Graham, D. E., & Gu, B. (2016). Effects of warming on
777 the degradation and production of low-molecular-weight labile organic carbon in an
778 Arctic tundra soil. *Soil Biology and Biochemistry*, 95, 202–211.
779 <https://doi.org/10.1016/j.soilbio.2015.12.022>
- 780 Yano, Y., Shaver, G. R., Giblin, A. E., Rastetter, E. B., & Nadelhoffer, K. J. (2010). Nitrogen
781 dynamics in a small arctic watershed: retention and downhill movement of ¹⁵N.
782 *Ecological Monographs*, 80(2), 331–351. <https://doi.org/10.1890/08-0773.1>
- 783 Ye, R., Jin, Q., Bohannan, B., Keller, J. K., McAllister, S. A., & Bridgham, S. D. (2012). pH
784 controls over anaerobic carbon mineralization, the efficiency of methane production, and
785 methanogenic pathways in peatlands across an ombrotrophic–minerotrophic gradient.
786 *Soil Biology and Biochemistry*, 54, 36–47. <https://doi.org/10.1016/j.soilbio.2012.05.015>
- 787 Yoo, K., Amundson, R., Heimsath, A. M., & Dietrich, W. E. (2006). Spatial patterns of soil
788 organic carbon on hillslopes: Integrating geomorphic processes and the biological C
789 cycle. *Geoderma*, 130(1–2), 47–65. <https://doi.org/10.1016/j.geoderma.2005.01.008>
- 790 Zalman, C., Keller, J. K., Tfaily, M., Kolton, M., Pfeifer-Meister, L., Wilson, R. M., et al.
791 (2018). Small differences in ombrotrophy control regional-scale variation in methane
792 cycling among Sphagnum-dominated peatlands. *Biogeochemistry*, 139(2), 155–177.
793 <https://doi.org/10.1007/s10533-018-0460-z>
- 794 Zheng, J., Thornton, P. E., Painter, S. L., Gu, B., Wullschleger, S. D., & Graham, D. E. (2019).
795 Modeling anaerobic soil organic carbon decomposition in Arctic polygon tundra: insights
796 into soil geochemical influences on carbon mineralization. *Biogeosciences*, 16(3), 663–
797 680. <https://doi.org/10.5194/bg-16-663-2019>
- 798 Zheng, J., Philben, M., Zhang, L., Jubb, A., Bill, M., Wullschleger, S. D., et al. (2019). Surface
799 and Active Layer Water Chemistry, Teller Road Mile Marker 27, Seward Peninsula,
800 Alaska, 2016–2018. Next Generation Ecosystem Experiments Arctic Data Collection,
801 Oak Ridge National Laboratory, U.S. Department of Energy, Oak Ridge, Tennessee,
802 USA. Retrieved October 1, 2019, from <https://doi.org/10.5440/1567181>

803

804

Figure 1.

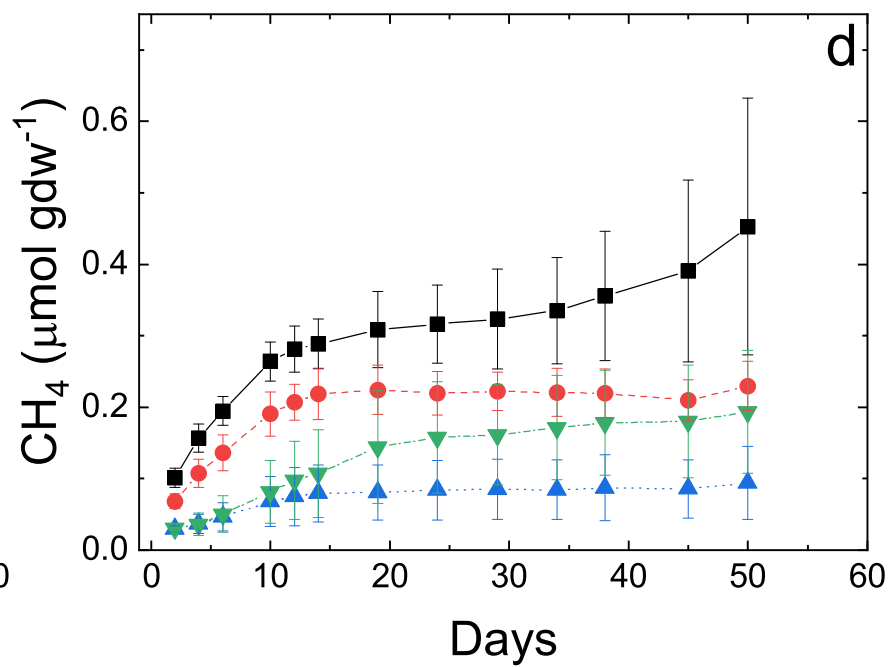
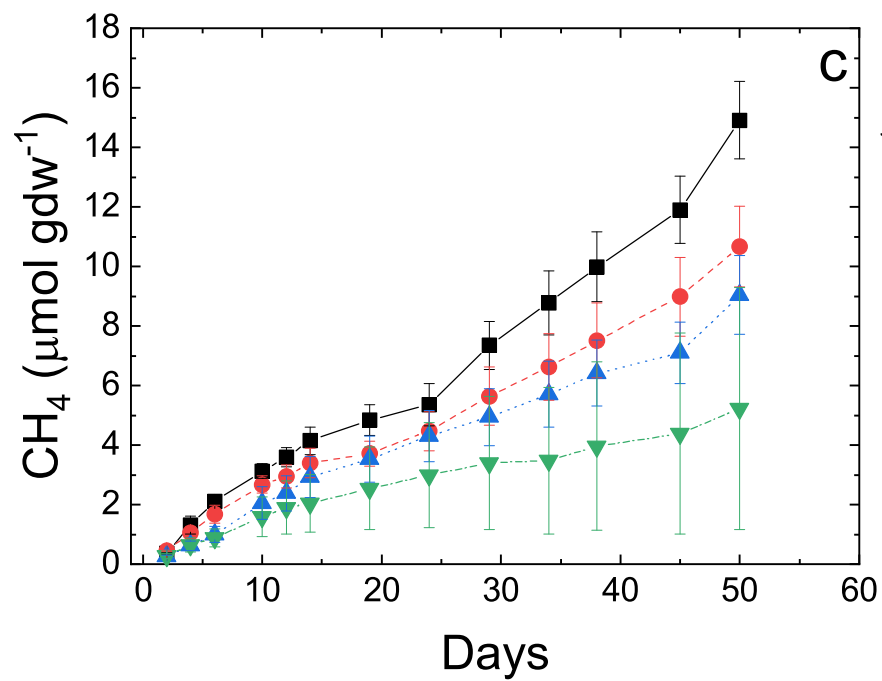
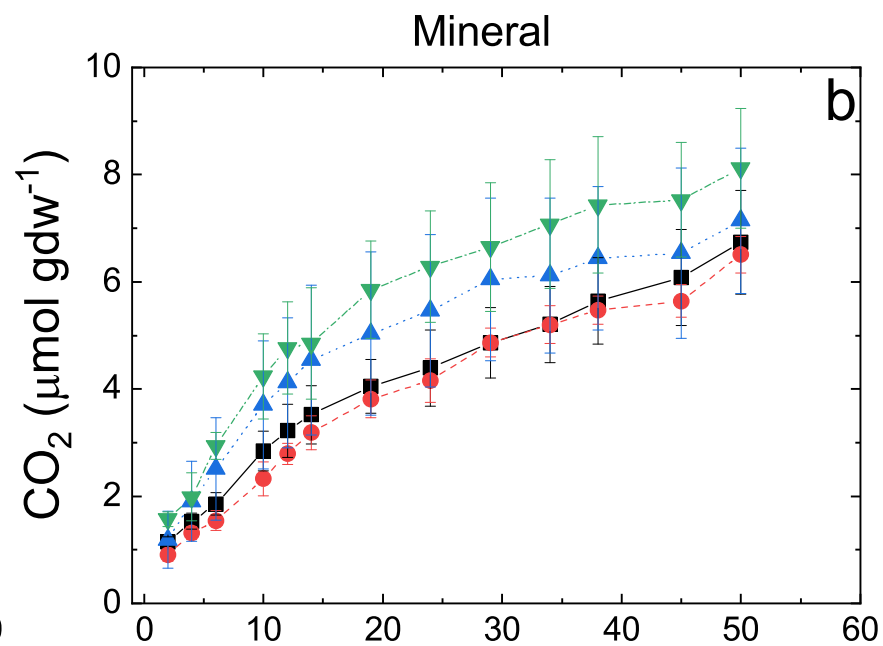
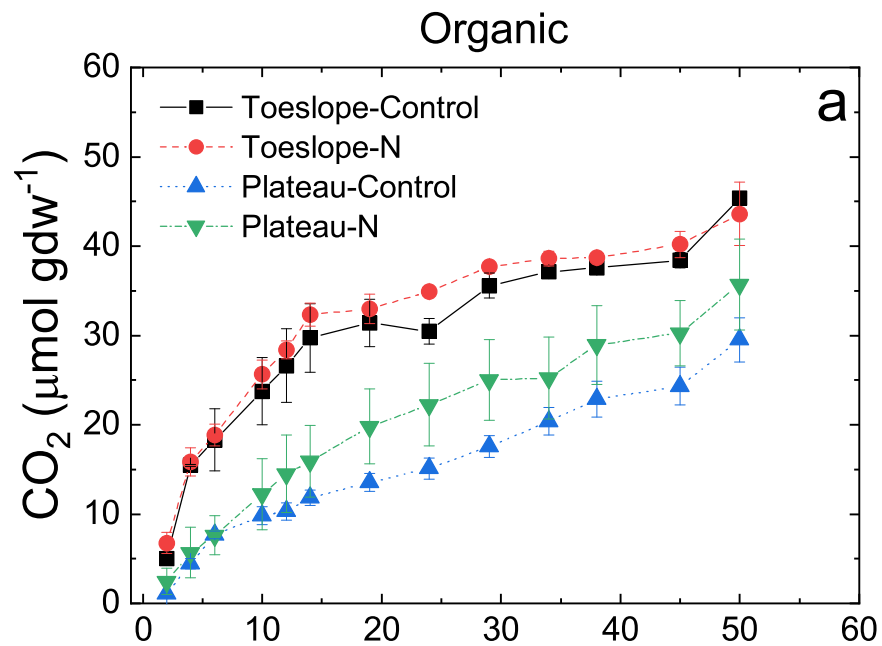


Figure 2.

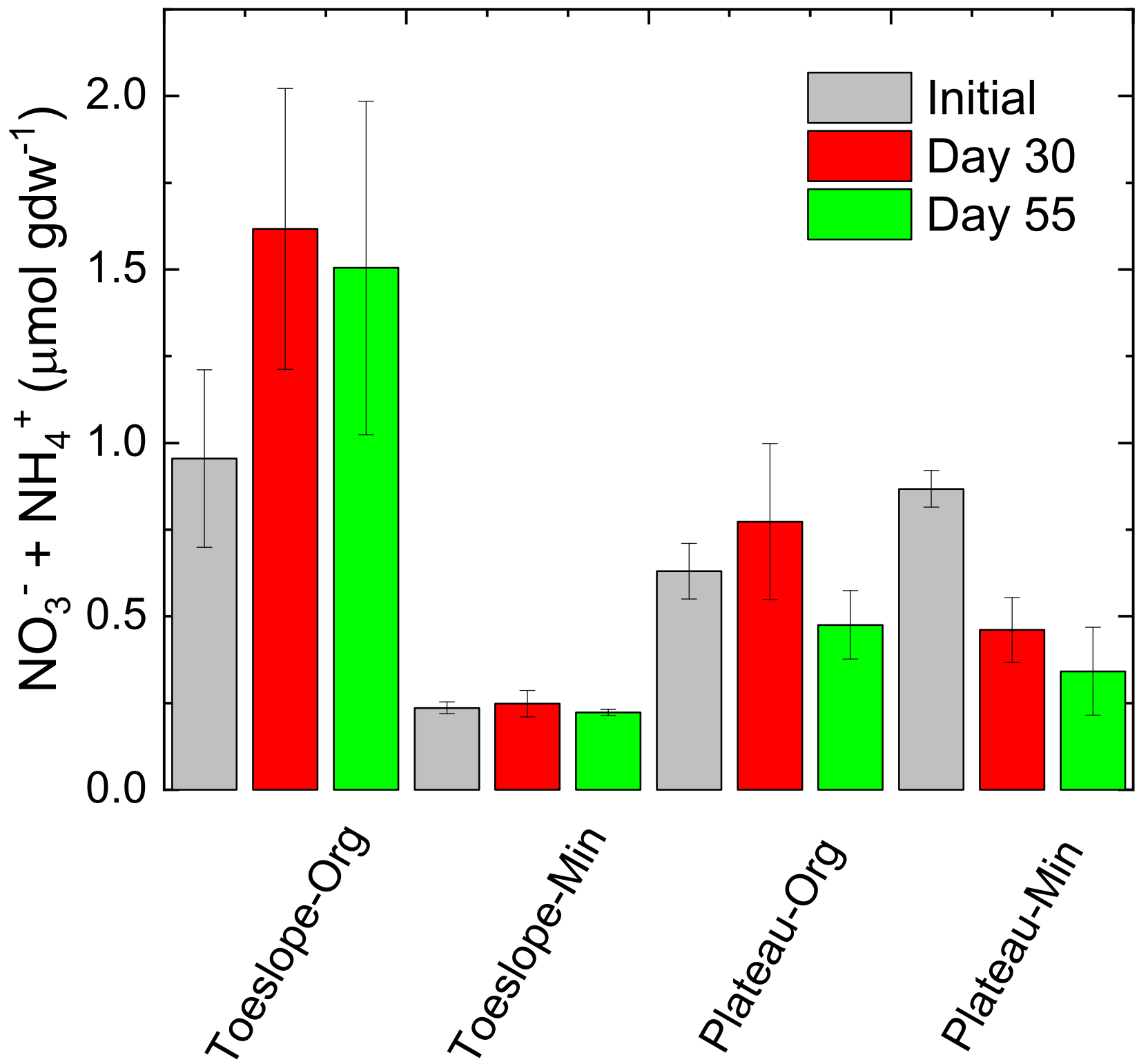


Figure 3.

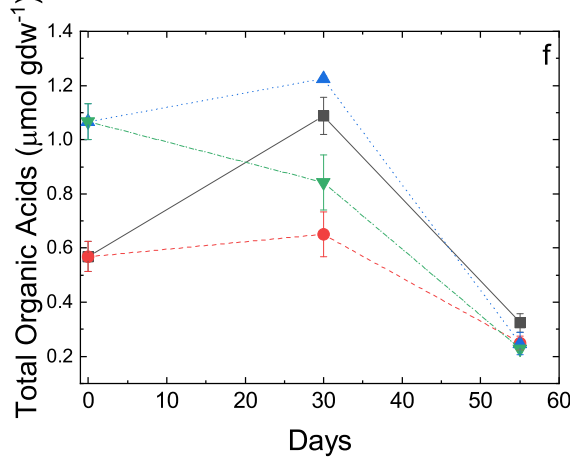
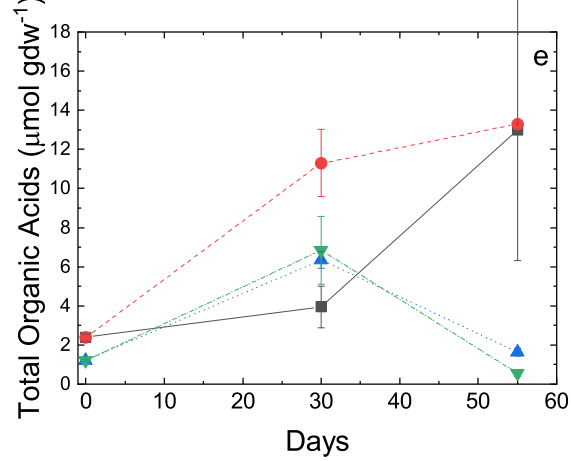
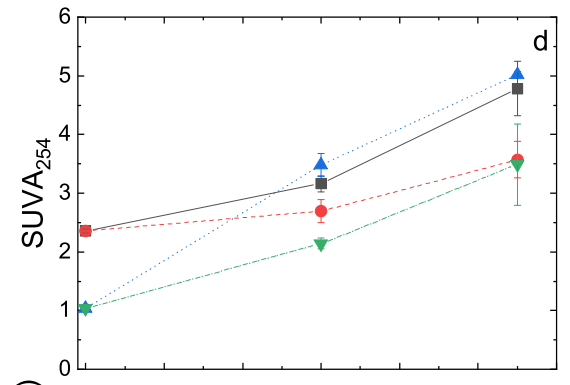
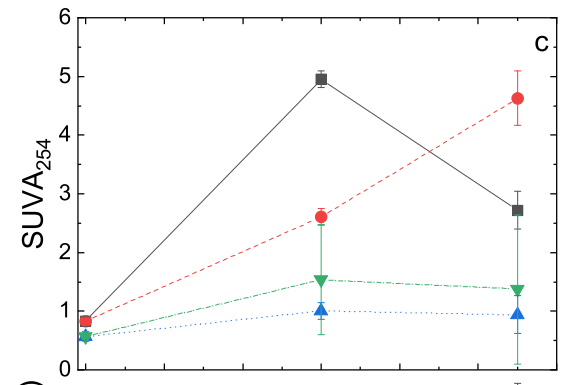
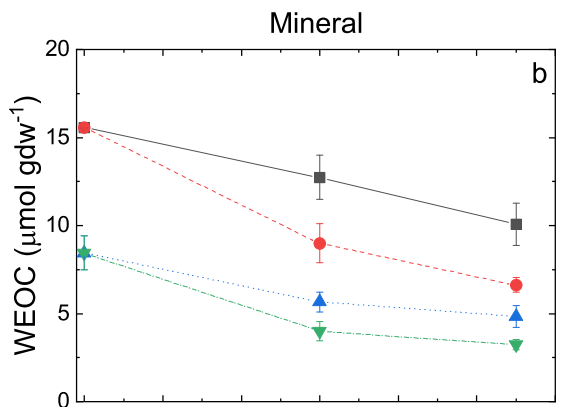
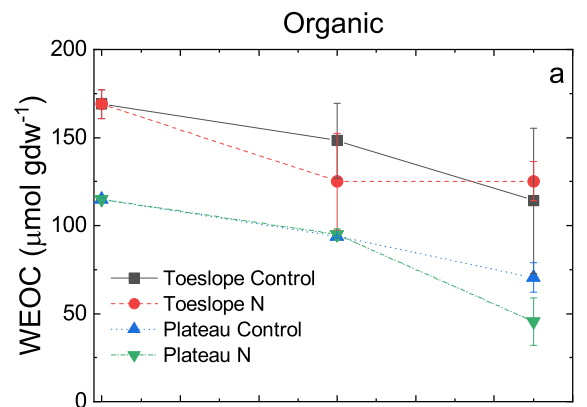


Figure 4.

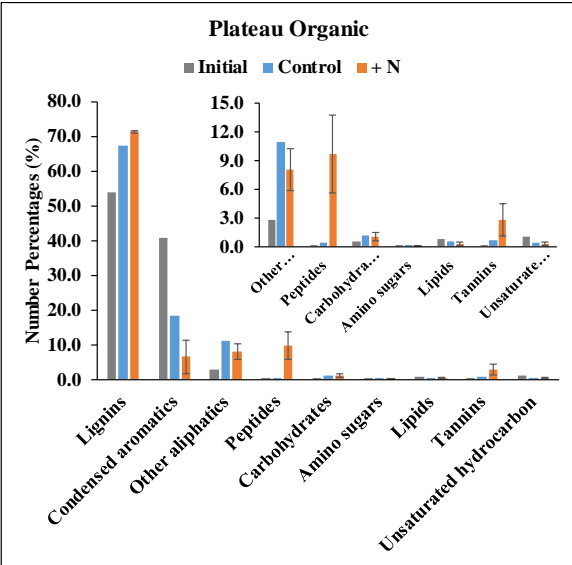
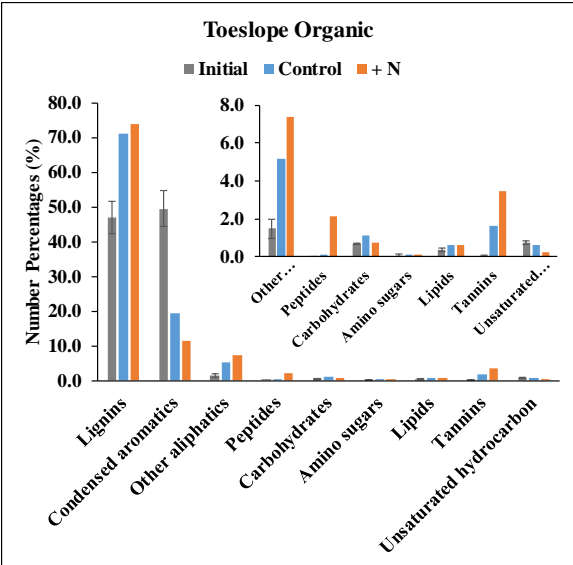
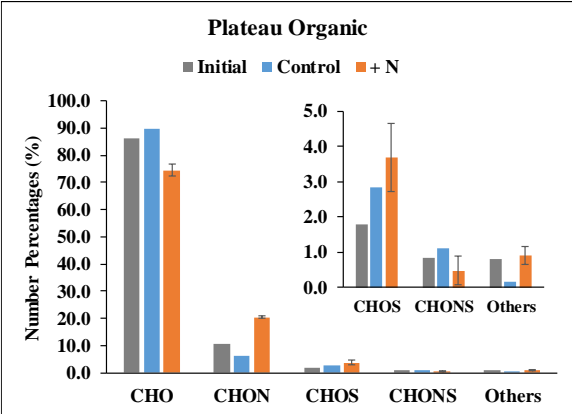
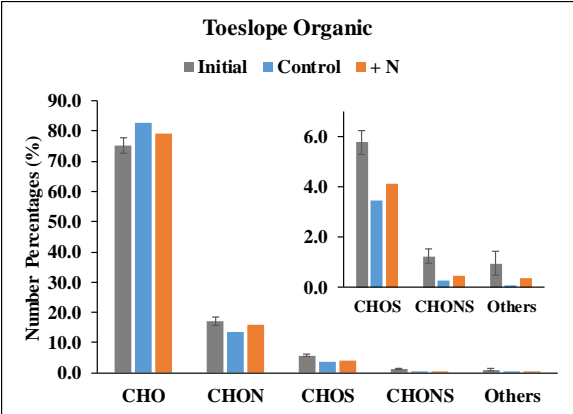


Figure 5.

